NACA RM E52B25

NACA

RESEARCH MEMORANDUM

ALTITUDE PERFORMANCE INVESTIGATION OF TWO FLAME-HOLDER AND FUEL-SYSTEM CONFIGURATIONS IN SHORT AFTERBURNER

By S. C. Huntley and H. D. Wilsted

Lewis Flight Propulsion Laboratory
Cleveland, Ohio

NATIONAL ADVISORY COMMITTEE
FOR AERONAUTICS
WASHINGTON

May 6, 1952
Declassified February 26, 1958

ERRATA No. 1

NACA RM E52B25

ALTITUDE PERFORMANCE INVESTIGATION OF TWO FLAME-HOLDER AND FUEL-SYSTEM CONFIGURATIONS IN SHORT AFTERBURNER

By S. C. Huntley and H. D. Wilsted

May 6, 1952

Page 33, figure 10: The curves are reversed. The solid curve should be dashed and the dashed curve should be solid.

Page 38, figure 15: The phrase "at rated turbine-outlet temperature" should be added to the legend.

NATIONAL ADVISORY COMMITTEE FOR AERONAUTICS

RESEARCH MEMORANDUM

ALTITUDE PERFORMANCE INVESTIGATION OF TWO FLAME-HOLDER AND FUEL-SYSTEM CONFIGURATIONS IN SHORT AFTERBURNER

By S. C. Huntley and H. D. Wilsted

SUMMARY

During an investigation in an altitude chamber, the altitude performance characteristics of two dissimilar flame-holder and fuel-system configurations were evaluated in a short afterburner. One configuration had a double annular V-gutter flame holder with fuel injectors located several inches upstream. The other had a double annular H-gutter flame holder and an additional annular V-gutter located a few inches downstream with the fuel injectors located immediately upstream of the H-gutter flame holder.

The altitude operating limits and the altitude performance of the V-gutter configuration were superior to those of the H-gutter configuration. At a Mach number of 0.6, the altitude limit of the V-gutter configuration was 50,000 feet as compared with 42,000 feet for the H-gutter configuration. The combustion efficiency was appreciably better for the V-gutter configuration; for example, at an altitude of 30,000 feet, the combustion efficiency at limiting turbine-outlet temperature was 74 percent for the V-gutter configuration as compared with 61 percent for the H-gutter configuration. As soon as fuel was introduced into the burner, spontaneous ignition was obtained with the V-gutter configuration to the maximum altitude at which ignition was attempted, 45,000 feet. Ignition of the H-gutter configuration required the use of a torch igniter.

INTRODUCTION

An investigation was conducted in an altitude chamber at the NACA Lewis laboratory to obtain a flame-holder and fuel-system configuration which would operate at high altitude in a short afterburner on an axial-flow turbojet engine. The afterburner shell used for this investigation was a production model furnished by the engine manufacturer.

The first part of the investigation was a brief evaluation of several types of flame-holder and fuel-injection systems (reference 1) to obtain an afterburner configuration that would meet the engine manufacturer's requirements for efficient operation at altitudes to at least 40,000 feet.

The configurations investigated could be separated into two distinct types: One type had a double-annular H-gutter type flame holder with a V-type gutter mounted several inches downstream. The fuel-injection system was mounted immediately upstream of the H-gutter flame holder and, therefore, did not provide a practical mixing length for evaporation of fuel and mixing of fuel and air. The other type consisted of a double-annular V-gutter type flame holder with the fuel-injection manifold located several inches upstream to provide a mixing length to evaporate the fuel and obtain additional mixing of fuel and air.

For the second phase of the investigation, one of the most promising configurations of each type was selected for further evaluation over a range of flight Mach numbers as well as altitude. In this phase of the program, the requirements were that satisfactory operation be obtained to an altitude of at least 50,000 feet.

The results of this complete evaluation of the altitude performance and operational characteristics of the two types of flame-holder and fuel-system configurations are reported herein. Operational limits of each configuration were determined for a wide range of simulated flight conditions and the performance characteristics were obtained at various altitudes for the complete operable range of afterburner fuel-air ratios. Comparative data are presented to show the performance variations with altitude at a flight Mach number of 0.6. Data are also presented to show the performance variation with flight Mach number of each configuration at the highest altitude where a reasonably wide range of afterburner fuel-air ratio could be obtained. The starting limits of both configurations at a flight Mach number of 0.6 are also discussed.

APPARATUS

Engine

An axial-flow-type turbojet engine with an afterburner was used in this investigation. With the afterburner inoperative, the engine has a static sea-level dry-thrust rating of 5100 pounds at rated engine speed, 7900 rpm, and at a turbine-outlet temperature of 1300° F. At this operating condition, the air flow is approximately 86 pounds per second and the fuel flow is 5740 pounds per hour. The over-all length

of the engine is approximately 195 inches and the maximum diameter is 43 inches. The main components of the engine are an 11-stage axial-flow compressor, eight cylindrical through-flow combustors, a single-stage turbine, and an afterburner.

Installation

The engine was installed in an altitude chamber as shown in figure 1. The altitude chamber is 10 feet in diameter and 60 feet long. A honeycomb is installed in the chamber upstream of the test section to provide smooth flow of the inlet air. The forward baffle separates the inlet air from the exhaust and provides a means of maintaining a pressure difference across the engine. A 14-inch butterfly valve, installed in the forward baffle, was used to provide cooling air for the engine compartment. The rear baffle acts as a radiation shield and prevents the recirculation of exhaust gases about the engine. The exhaust gas from the jet nozzle was discharged into an exhaust diffuser. The pressure rise in this diffuser assisted in simulating an altitude pressure in the test section. Combustion in the afterburner was observed through a periscope located in the exhaust duct behind the engine.

Afterburner

A drawing of the afterburner assembly including the inlet diffuser is shown in figure 2 with a typical flame-holder and fuel-injection system installed. The afterburner had an inlet diameter of 31 inches and an over-all length including the variable-area exhaust nozzle of $47\frac{1}{2}$ inches, giving a length-diameter ratio of only 1.53. The variable-area nozzle was a two-position clamshell-type nozzle. During afterburning, the exhaust nozzle was in the open position and the area was approximately 357 square inches. In the closed position, the exhaust-nozzle area was adjusted to give rated turbine-outlet temperature at rated engine speed. Fuel was supplied to the afterburner by an air-turbine fuel pump which was driven by air bled from the compressor outlet.

Cooling of the burner section was accomplished by an ejector cooling shroud. The exhaust jet discharging through this shroud induced a flow of cooling air over the burner shell. The air entered the cooling shroud from the test section of the altitude chamber at approximately the simulated altitude ambient pressure and at a temperature of approximately 100° F.

Configurations

The installations of the two configurations used in this investigation are shown in figure 3. The H-gutter flame holder with a trailing V-gutter and the close-coupled fuel system are designated as configuration A. The V-gutter flame holder with the upstream fuel system is designated configuration B.

Configuration A. - The flame holder of configuration A consisted of two annular H-sections connected by eight radial H sections with a trailing V-section. Critical dimensions of the flame holder are shown in figure 3(a). Orifices in the cross member of the H sections metered fuel and air to the sheltered zone of the gutters. The fuel-injection manifold consisted of three concentric rings connected by four radial tubes. Also, the two outer rings were connected by 12 additional tubes. Fuel orifices were located in the rings and connecting tubes to provide injection in an upstream direction but at an angle to the gas flow. The location of the fuel orifices is shown in figure 4(a).

Configuration B. - The flame holder consisted of two annular, staggered V-sections with six radial interconnecting V-sections. Dimensions of the flame holder are shown in figure 3(b). The fuel-injection manifold consisted of 12 radial tubes connected by an outer and an inner ring. Fuel orifices were located in the radial tubes only and placed to provide a uniform radial distribution of fuel (see fig. 4(b)).

Ignition system. - The same afterburner ignition system was provided for both configurations. Ignition was provided by a momentary increase in fuel flow to one of the engine combustors (see reference 2). This excess fuel in one combustor caused a burst of flame through the turbine and ignition in the afterburner.

Instrumentation

Pressures and temperatures were measured at stations throughout the engine and afterburner (fig. 1(b)). Compressor air flow was determined by the use of survey rakes mounted at the engine inlet, station 1. Instrumentation was installed for measuring both the engine midframe air-bleed and the air bled from the compressor outlet that was used to drive the air turbine of the afterburner fuel pump. These air flows were subtracted from the compressor air flow to obtain the afterburner air flow. Afterburner-inlet total pressure and temperature were determined from a survey at the turbine outlet (station 5, fig. 5(a)). Static-pressure measurements were obtained with three wall orifices located at the burner inlet (station 6, fig. 1(b)). Total pressures were measured at the exhaust-nozzle inlet with a water-cooled survey

rake (station 7, fig. 5(b)). Ambient pressure in the region of the exhaust-nozzle outlet was determined by static probes in the plane of the nozzle exit (station 8) and altitude pressure by static probes in the plane of the shroud exit (station 0). Engine and afterburner fuel flows were measured by calibrated rotameters.

Procedure

The altitude operational limits of each configuration were determined for a range of flight Mach numbers from 0.4 to 1.0. The minimum fuel flow at each flight condition was determined by imminent blow-out and the maximum fuel flow was determined by either rated turbine-outlet temperature or rich blow-out. The maximum operable altitude was determined by increasing altitude and holding the fuel flow and the flight Mach number constant until blow-out occurred.

Performance data were obtained for altitudes from 10,000 to 45,000 feet for a flight Mach number of 0.6 with both configurations. Also, performance data were obtained for flight Mach numbers of 0.4 to 1.0 at an altitude of 30,000 feet with configuration A and at an altitude of 40,000 feet with configuration B. Performance data at each flight condition were obtained at several afterburner fuel flows at rated engine speed.

Starting data were obtained at a flight Mach number of 0.6. The starting technique consisted in supplying fuel to the afterburner with the exhaust nozzle in the closed position. If autoignition was obtained, the jet nozzle was opened to the afterburning position. If autoignition was not obtained, the torch fuel flow was turned on for a period not exceeding 2 seconds. When ignition took place, the jet nozzle was quickly opened and the torch fuel flow was shut off. Afterburner ignition was investigated over the operable fuel-air ratio range of the afterburner by presetting fuel flows to those corresponding to the steady-state afterburner operation.

The engine-inlet air for each flight condition was supplied at the total temperature and total pressure corresponding to NACA standard atmospheric conditions; 100-percent ram-pressure recovery at the engine inlet was assumed. The symbols used in this report and the methods used to compute the performance parameters are presented in the appendix.

Two fuel-air ratios are defined and used in computing and presenting the results of the investigation:

(1) The afterburner fuel-air ratio $(f/a)_t$ is defined as the ratio of the afterburner fuel flow to the engine air flow (air flow

entering compressor minus air bled from compressor). This fuel-air ratio was used when only the flight condition, the engine speed, and the afterburner fuel flow were recorded. The air flow values were taken from the engine air-flow calibration curves.

(2) The unburned-air afterburner fuel-air ratio $(f/a)_{ua}$ is defined as the ratio of the afterburner fuel flow to the unburned air flow entering the afterburner (engine air flow minus the air burned in the engine). This fuel-air ratio was used when complete performance data were recorded.

The fuel used in this investigation was MIL-F-5624A, grade JP-3, having a lower heating value of 18,680 Btu per pound and a hydrogen-carbon ratio of 0.172.

RESULTS AND DISCUSSION

Operational Limits

The afterburner operable range of fuel-air ratios is shown for both configurations in figure 6 as a function of altitude for flight Mach numbers from 0.4 to 1.0. For both configurations at a flight Mach number of 0.6, minimum and maximum fuel-air ratios increased with altitude resulting in no great change in operable range of fuel-air ratio except near the altitude limits where they converged. The data indicate that the trends would be the same for other flight Mach numbers. During the determination of the maximum altitude limits, complete data were not obtained and it was quite possible to exceed the rated turbine-outlet temperature. The rated turbine-outlet-temperature lines were based on subsequent performance data.

As the fuel-air ratio increased near limiting altitudes for configuration A, a rich blow-out occurred before rated turbine-outlet temperature was reached (fig. 6(a)). Conversely, with configuration B, the maximum fuel-air-ratio operable limit was generally established not by blow-out but when the maximum allowable turbine-outlet temperature was reached (fig. 6(b)).

The effect of increasing flight Mach number on the operational limits of the two configurations is shown in figure 6 as a general upward shift in the altitude operational limit. The variation of altitude limit with increasing flight Mach number is shown in figure 7(a). The maximum operable altitude of both configurations increased at about the same rate with flight Mach number but that of configuration B was 6000 to 9000 feet higher than that of configuration A. At a flight Mach number of 0.6, the altitude limits were about 42,000 and 50,000 feet for configurations A and B, respectively. The variation of

fuel-air-ratio limit with increasing flight Mach number at an altitude of 40,000 feet is shown in figure 7(b). Configuration A would not operate below a flight Mach number of 0.5, and the operable range of fuel-air ratio, which was limited by blow-out, increased with flight Mach number. The operable range of fuel-air ratio for configuration B was about the same over the range of flight Mach numbers investigated. The decrease in fuel-air ratio of configuration B with increasing flight Mach number is a result of increasing combustion efficiency. Also, the lower operating fuel-air ratios for configuration B result from higher combustion efficiency. The leaner fuel-air ratios and higher operating limits of configuration B indicate the combined advantage of uniform circumferential fuel distribution, greater mixing length between fuel injection station and flame holders, and V-gutter instead of H-gutter flame holders.

Performance Characteristics

Effect of altitude. - The performance data are presented in table I and are shown graphically in figures 8 to 12 for a flight Mach number of 0.6, rated engine speed, and several altitudes. The variation in afterburner-inlet conditions with afterburner fuel-air ratio is presented in figure 8. The fuel-air ratio used here is based on the unburned air available at the afterburner inlet as defined in the Procedure section. The turbine-outlet temperature and turbine-outlet pressure increased with increasing fuel-air ratio, as expected for operation with a constant-area jet nozzle. At a given fuel-air ratio, the turbine-outlet temperature and the turbine-outlet pressure decreased with increasing altitude approximately in proportion to the decrease in engine-inlet temperature and pressure. The burner-inlet velocity varied only slightly with fuel-air ratio, decreasing from about 400 feet per second to about 385 feet per second from the minimum to maximum operable fuel-air ratio.

The variation of exhaust-gas total temperature and afterburner combustion efficiency with afterburner fuel-air ratio is shown in figure 9 for the altitudes investigated. At a given fuel-air ratio, the exhaust-gas total temperature decreased with increasing altitude primarily because of a decrease in afterburner combustion efficiency (fig. 9(b)) and to a lesser extent because of decreased turbine-outlet temperatures (fig. 8(b)).

The rich fuel-air-ratio limit of operation, as determined by limiting turbine-outlet temperature (maximum thrust), occurred near the peak of the afterburner-efficiency curves at an altitude of 10,000 feet. With increasing altitude, this rich limit for both configurations occurred at fuel-air ratios progressively greater than that for peak combustion efficiency. The combustion efficiencies at limiting

turbine-outlet temperature for configuration A were 81 percent at 10,000 feet and 61 percent at 30,000 feet. The corresponding efficiencies of configuration B were 88 and 74 percent, respectively. The effect of altitude on combustion efficiency is shown graphically in figure 10 for a flight Mach number of 0.6. Although both configurations show a rapid decrease in combustion efficiency with increasing altitude, configuration B had a 7 to 13 percent higher combustion efficiency than configuration A.

Flame holders such as configuration B with uniform fuel distribution were capable of operation at high altitude without decrease in maximum burner efficiency (reference 1). The unexpected drop in maximum efficiency at altitude for configuration B was probably due to a less uniform fuel distribution than was obtained with better configurations in reference 1. Because the fuel was injected 45° upstream instead of normal to the stream, there was less tendency to distribute fuel completely across the stream, especially at the lower fuel flows corresponding to the higher altitudes.

The variation in net thrust and net thrust specific fuel consumption with altitude and fuel-air ratio is shown in figure 11 for both configurations. A cross plot of the net thrust at rated turbine-outlet temperatures is presented in figure 12(a) and is, of course, essentially equal for the two configurations. Because the rated turbine-outlet temperatures occurred at lower fuel-air ratio for configuration B than for configuration A, the net thrust specific fuel consumption (fig. 12(b)) was lower for configuration B. At an altitude of 30,000 feet, the net thrust specific fuel consumption for configuration A was 2.62 whereas that of configuration B was 2.33. As altitude increased, an even greater advantage of configuration B was evident.

Effect of flight Mach number. - The variation of afterburner performance at rated engine speed, with flight Mach number and fuel-air ratio, is shown in figures 13 to 17. Performance of configuration B was investigated at an altitude of 40,000 feet and flight Mach numbers of 0.4, 0.6, 0.8, and 1.0. Later when the performance of configuration A was investigated, it was found that operation of the afterburner could not be obtained at any fuel-air ratio at a flight Mach number of 0.4 at 40,000-foot altitude and operation at a flight Mach number of 0.6 was possible only over a very limited range of fuel-air ratios (fig. 6). The performance calibration of configuration B was therefore conducted at 30,000 feet altitude. The data for the two configurations then represent the altitudes at which performance at flight Mach numbers from 0.4 to 1.0 could be obtained over a range of fuel-air ratios with stable combustion.

The variation in afterburner-inlet conditions with flight Mach number and fuel-air ratio is presented in figure 13. The afterburner-inlet velocity (fig. 13(a)) is relatively unaffected by flight Mach number but shows the same small decrease with increasing fuel-air ratio previously discussed. The turbine-outlet gas temperature (fig. 13(b)) and the turbine-outlet pressure (fig. 13(c)) increased with increasing flight Mach number. This increase in turbine-outlet gas temperature and pressure is not quite proportional to the increase in engine-inlet temperature and pressure with increasing flight Mach number because of a secondary effect due to compressor Reynolds number.

The afterburner combustion efficiency and exhaust-gas temperature are shown in figure 14. The increase in exhaust-gas temperature (fig. 14(a)) with increasing flight Mach number results primarily from the increased combustion efficiency (fig. 14(b)). The combustion efficiency rises with increasing flight Mach number because of the increased burner-inlet pressure and temperature (fig. 13). For both configurations, the maximum combustion efficiency for each flight Mach number investigated occurred at a fuel-air ratio of about 0.03. The effect of flight Mach number on afterburner efficiency at rated turbine-outlet temperature is shown in figure 15 (a cross plot of fig. 14(b)). At flight Mach numbers above 0.7, the afterburner efficiency of configuration B at 40,000 feet was about the same as the afterburner efficiency of configuration A at 30,000 feet. Below a flight Mach number of 0.7, the sensitivity of configuration A to flight Mach number was far more pronounced than that of configuration B even with the lower altitude advantage.

The variation of over-all engine performance is presented in figure 16 as a function of afterburner fuel-air ratio for several flight Mach numbers. Net thrust increased (fig. 16(a)) and net thrust specific fuel consumption (fig. 16(b)) decreased slightly with increasing flight Mach number. The net thrust increased with increasing flight Mach number primarily because of the accompanying higher air flows. The lowered specific fuel consumption with increasing flight Mach number resulted primarily from the higher cycle and combustion efficiencies. Figure 17 is a cross plot of the net thrust specific fuel consumption at limiting turbine-outlet temperature. Although configuration B was operated at the higher altitude (40,000 ft), it provided the lower net thrust specific fuel consumption throughout the range of flight Mach numbers investigated.

Ignition Characteristics

As previously discussed, two methods of ignition, (1) autoignition and (2) torch ignition, were used to initiate combustion in the afterburner. The range of altitudes and afterburner fuel-air ratios $(f/a)_t$

over which ignition was obtained is shown in figure 18 for a flight Mach number of 0.6. The dashed curves are the operational limits of the two burner configurations from figure 6. Because the fuel flow was measured at the moment ignition occurred, before fuel flow had stabilized, accurate fuel-air ratios cannot be expected for the starting data. Autoignition was obtained with configuration B throughout the operational range of fuel-air ratios to an altitude of 45,000 feet, the highest altitude at which afterburner ignition was attempted. Autoignition could not be obtained with configuration A possibly because of the cooling of the flame holder by the impingement of unvaporized fuel from the closely coupled fuel manifold. With configuration A, the afterburner could be ignited by the torch method throughout the operable fuel-air-ratio range to an altitude of at least 30,000 feet. Two out of three attempts to obtain ignition were successful at a lean fuel-air ratio at 35,000 feet.

CONCLUDING REMARKS

An investigation of the altitude performance of two flame-holder and fuel-system configurations in a short afterburner has been conducted on an axial-flow turbojet engine in an altitude chamber. One configuration consisted of a double annular H-gutter flame holder having an additional V-gutter several inches downstream. The fuel injection manifold was located directly upstream of the H-gutter flame holder. The other configuration had a double annular V-gutter flame holder with the fuel-injection manifold mounted several inches upstream. This arrangement allowed more time for vaporization of the fuel and mixing of the fuel and air. The double annular V-gutter configuration provided the better altitude performance and operating characteristics. At a flight Mach number of 0.6, the altitude limits were about 42,000 and 50,000 feet for the H-gutter and V-gutter afterburner configurations, respectively. The respective combustion efficiencies of the two configurations at limiting turbine-outlet temperature and at an altitude of 30,000 feet and a flight Mach number of 0.6 were 61 and 74 percent. At these operating conditions, the improved combustion efficiency reduced the afterburner net thrust specific fuel consumption from 2.62 to 2.33 pounds of fuel per pound of net thrust.

Ignition of the V-gutter configuration afterburner occurred spontaneously when the fuel was introduced into the afterburner. This autoignition was possible to an altitude of 45,000 feet, the highest altitude at which ignition was attempted. Ignition of the H-gutter configuration, however, was not spontaneous and the use of a torch igniter was required.

The superiority of the V-gutter configuration in the short afterburner is attributed to (1) improved circumferential fuel distribution, (2) increased fuel mixing and vaporization time, and (3) use of the V-gutter flame holder with its superior flame-holding characteristics.

Lewis Flight Propulsion Laboratory
National Advisory Committee for Aeronautics
Cleveland, Ohio

APPENDIX - METHODS OF CALCULATION

Symbols

The following symbols are used in this report:

A	area, sq ft
C_d	flow (discharge) coefficient, ratio of effective flow area to measured area
C_T	thermal expansion ratio, ratio of hot exhaust-nozzle-throat area to cold exhaust-nozzle-throat area
$C_{V,e}$	effective velocity coefficient, ratio of actual jet thrust to calculated jet thrust
F	thrust, lb
f/a	fuel-air ratio
g	acceleration due to gravity, 32.174 ft/sec^2
h_a	enthalpy, Btu/lb
h_c	lower heating value of fuel based on reference temperature, Btu/lb
M	Mach number
N	engine speed, rpm
P	total pressure, lb/sq ft
p	static pressure, lb/sq ft
R	gas constant, 53.3 ft-lb/(lb)($^\circ$R)
T	total temperature, $^\circ$R
T_r	reference temperature, 540° R
V	velocity, ft/sec
W_a	air flow, lb/sec
W_f	fuel flow, lb/hr

W_g gas flow, lb/sec

γ ratio of specific heats

η combustion efficiency

Subscripts:

c calculated

e engine

i indicated

j jet

n net

t afterburner

ua unburned air

0 free-stream ambient conditions

1 engine inlet

3 compressor outlet

5 turbine outlet (diffuser inlet)

6 afterburner inlet

7 exhaust-nozzle inlet

8 exhaust-nozzle throat

Methods of Calculation

Flight speed and Mach number. - The simulated flight speed and Mach number at which the engine and afterburner were operated were determined from the following equations:

$$V_0 = \sqrt{gRT_1 \frac{2\gamma_1}{\gamma_1 - 1}\left[1 - \left(\frac{p_0}{p_1}\right)^{\frac{\gamma_1 - 1}{\gamma_1}}\right]} \qquad (1)$$

$$M_0 = \sqrt{\frac{2}{\gamma_1 - 1}\left[\left(\frac{P_1}{P_0}\right)^{\frac{\gamma_1 - 1}{\gamma_1}} - 1\right]} \tag{2}$$

where γ was assumed to be 1.4 and the total temperature was assumed to be equal to the indicated temperature inasmuch as the thermocouple recovery factor was 0.96.

Gas flow. - The compressor-inlet air flow was computed as

$$W_{a,1} = A_1 P_1 \sqrt{\frac{g}{RT_1}} \sqrt{\frac{2\gamma_1}{\gamma_1 - 1}\left(\frac{P_1}{p_1}\right)^{\frac{\gamma_1 - 1}{\gamma_1}}\left[\left(\frac{P_1}{p_1}\right)^{\frac{\gamma_1 - 1}{\gamma_1}} - 1\right]} \tag{3}$$

The engine air flow at station 3 was calculated by subtracting the midframe air-bleed and the air flow required to drive the afterburner fuel pump from the compressor inlet air flow. The midframe air-bleed and afterburner fuel-pump air flow were calculated in a similar manner to the compressor-inlet air flow. The total gas flow at the turbine outlet was calculated as

$$W_{g,5} = W_{a,3} + \frac{W_{f,e}}{3600} \tag{4}$$

The total gas flow at the exhaust-nozzle throat was calculated as

$$W_{g,8} = W_{g,5} + \frac{W_{f,t}}{3600} \tag{5}$$

Turbine-outlet total temperature. - The turbine-outlet total temperature was corrected for impact.

$$T_5 = \frac{T_{5,i}\left(\frac{P_5}{p_5}\right)^{\frac{\gamma_5 - 1}{\gamma_5}}}{1 + 0.95\left[\left(\frac{P_5}{p_5}\right)^{\frac{\gamma_5 - 1}{\gamma_5}} - 1\right]} \tag{6}$$

The value 0.95 is the thermocouple recovery factor.

Afterburner inlet velocity. - The continuity equation was used to calculate the afterburner inlet velocity. The static pressure and area were measured at station 6. The total-pressure and -temperature measurements from station 5 were used and it was assumed that there was no loss between the two stations.

$$V_6 = \frac{W_{g,5}\, RT_5}{A_6 p_6} \left(\frac{p_6}{P_5}\right)^{\frac{\gamma_6 - 1}{\gamma_6}} \tag{7}$$

Afterburner fuel-air ratio. - Two afterburner fuel-air ratios are used in this report and are defined as follows:

(1) The ratio of the afterburner fuel flow to engine air flow,

$$\left(\frac{f}{a}\right)_t = \frac{W_{f,t}}{3600\ W_{a,3}} \tag{8}$$

(2) The ratio of the afterburner fuel flow to the unburned air entering the afterburner,

$$\left(\frac{f}{a}\right)_{ua} = \frac{W_{f,t}}{3600\ W_{a,3} - \frac{W_{f,e}}{0.0672}} \tag{9}$$

The assumption used in obtaining this equation was that the fuel injected in the engine was completely burned. The value of 0.0672 is the stoichiometric fuel-air ratio for the fuel used.

Exhaust-gas total temperature. - The exhaust-gas total temperature was determined by

$$T_8 = \frac{2g}{R} \left(\frac{A_8 C_d C_T p_8}{W_{g,8}}\right)^2 \left(\frac{\gamma_8 - 1}{\gamma_8}\right) \left(\frac{P_7}{p_8}\right)^{\frac{\gamma_8 - 1}{\gamma_8}} \left[\left(\frac{P_7}{p_8}\right)^{\frac{\gamma_8 - 1}{\gamma_8}} - 1\right] \tag{10}$$

The flow coefficient C_d was obtained from reference 3. The exhaust-nozzle-throat area A_8 was measured at room temperature. Values of the thermal expansion ratio C_T of the exhaust nozzle were determined from the thermal expansion coefficient for the exhaust-nozzle material and the measured skin temperature.

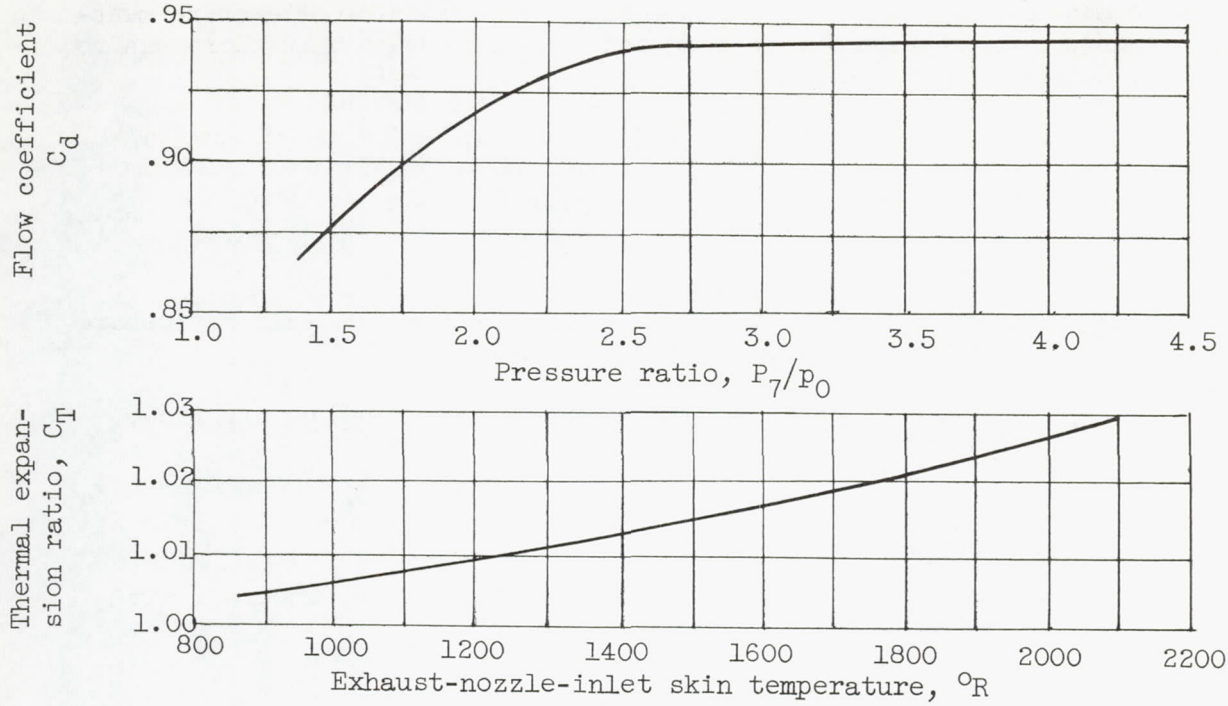

Exhaust-nozzle-throat static pressure p_8 was determined as follows:

$$p_8 = p_0 \quad \text{for subsonic flow}$$

$$p_8 = P_7 \left(\frac{2}{\gamma_8+1}\right)^{\frac{\gamma_8}{\gamma_8-1}} \quad \text{for sonic flow}$$

Afterburner combustion efficiency. - The afterburner combustion efficiency was calculated from

$$\eta_t = \frac{h_a\Big]_1^8 + \left[\left(\frac{f}{a}\right)_e + \left(\frac{f}{a}\right)_t\right]\frac{Am+B}{m+1}\Bigg]_{T_r}^8 - \eta_e\left(\frac{f}{a}\right)_e h_c}{h_c\left[\left(\frac{f}{a}\right)_t + \left(\frac{f}{a}\right)_e (1-\eta_e)\right]} \qquad (11)$$

The engine fuel was not assumed to be burned completely in the engine. The unburned engine fuel was charged to the afterburner. The engine combustion efficiency was 0.96; this value was obtained from an altitude calibration of a similar engine. The term $\frac{Am+B}{m+1}$ accounts for the difference between the enthalpy of the carbon dioxide and water vapor in the burned mixture and the enthalpy of the oxygen removed from the air by their formation (reference 4). Dissociation was not considered inasmuch as its effect is negligible for temperatures to 3200° R.

Thrust. - The jet thrust was calculated from

$$F_j = C_{v,e}\left[W_{g,8}\sqrt{\frac{RT_8}{g}\frac{2\gamma_8}{\gamma_8-1}\left[1-\left(\frac{p_8}{P_7}\right)^{\frac{\gamma_8-1}{\gamma_8}}\right]}+A_8C_T\,(p_8-p_0)\right] \quad (12)$$

The values of p_8 and C_T are explained in the discussion of equation (10). The effective velocity coefficient $C_{v,e}$ was obtained from reference 1.

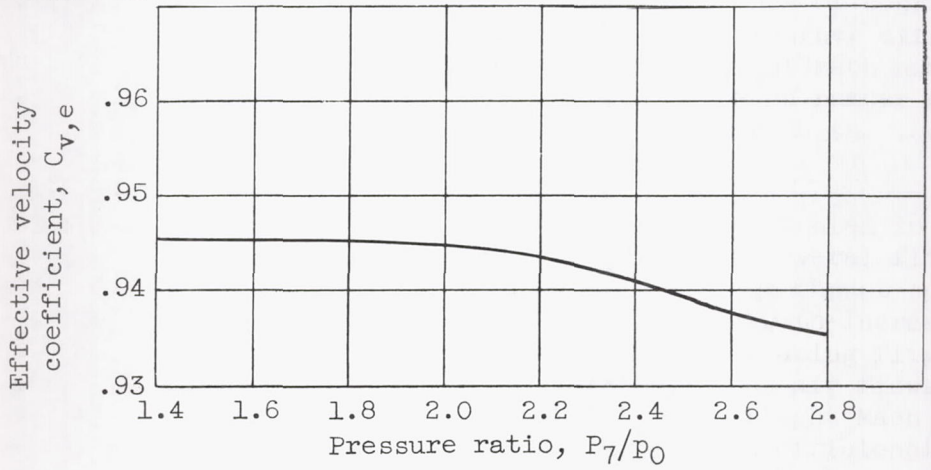

Net thrust was obtained from the jet thrust by

$$F_n = F_j - \frac{W_{a,1}}{g}V_0 \quad (13)$$

Net thrust specific fuel consumption. - The net thrust specific fuel consumption was calculated from

$$\frac{W_f}{F_n} = \frac{W_{f,e} + W_{f,t}}{F_n} \quad (14)$$

REFERENCES

1. Grey, Ralph E., Krull, H. G., and Sargent, A. F.: Altitude-Investigation of 16 Flame-Holder and Fuel-System Configurations in Tail-Pipe Burner. NACA RM E51E03, 1951.

2. Fleming, W. A., Conrad, E. William, and Young, A. W.: Experimental Investigation of Tail-Pipe-Burner Design Variables. NACA RM E50K22, 1951.

3. Grey, Ralph E., Jr., and Wilsted, H. Dean: Performance of Conical Jet Nozzles in Terms of Flow and Velocity Coefficients. NACA Rep. 933, 1949. (Formerly NACA TN 1757.)

4. Turner, L. Richard, and Bogart, Donald: Constant-Pressure Combustion Charts Including Effects of Diluent Addition. NACA Rep. 937, 1949. (Formerly NACA TN's 1086 and 1655.)

TABLE I - PERFORMANCE

Run	Flight Mach number M_0	Altitude (ft)	Engine speed N (rpm)	Afterburner fuel flow $W_{f,t}$ (lb/hr)	Engine fuel flow $W_{f,e}$ (lb/hr)	Jet thrust F_J (lb)	Net thrust F_n (lb)	Air flow W_a (lb/sec)	Net thrust specific fuel consumption $\frac{W_{f,t} + W_{f,e}}{F_n}$ (lb/(hr) (lb thrust))	Afterburner fuel-air ratio $(f/a)_t$	Afterburner fuel-air ratio $(f/a)_{ua}$	Afterburner inlet velocity V_6 (ft/sec)
					CONFIGURATION A							
1	0.4	30,000	7921	1659	1647	1882	1472	30.58	2.245	0.0151	0.0194	395.2
2			7919	2285	1908	2318	1917	30.53	2.187	.0208	.0280	379.8
3			7922	2795	2033	2474	2065	30.36	2.338	.0256	.0353	378.7
4			7918	3350	2083	2581	2169	30.78	2.505	.0302	.0419	383.5
5			7914	3985	2079	2534	2133	30.12	2.843	.0368	.0514	384.5
6	0.6	10,000	7915	2770	3373	4306	2779	71.95	2.211	0.0107	0.0133	402.6
7			7922	3885	3940	5145	3645	72.08	2.147	.0150	.0193	395.9
8			7911	5030	4297	5730	4235	72.09	2.202	.0194	.0257	394.4
9			7922	6300	4632	6236	4728	72.16	2.312	.0243	.0330	393.4
10		20,000	7914	1827	2213	2750	1713	51.39	2.358	0.0099	0.0120	410.9
11			7920	2300	2500	3201	2161	51.39	2.221	.0124	.0156	403.1
12			7919	3160	2934	3858	2833	51.26	2.151	.0171	.0224	394.4
13			7911	4040	3160	4228	3208	50.78	2.244	.0221	.0297	387.5
14			7917	5125	3427	4545	3522	50.84	2.428	.0280	.0388	388.7
15		30,000	7938	1671	1720	2120	1430	34.89	2.371	0.0133	0.0167	413.7
16			7924	2030	1931	2515	1845	33.97	2.147	.0166	.0217	393.8
17			7918	2870	2222	2914	2249	34.24	2.264	.0233	.0318	389.5
18			7915	3770	2344	3132	2450	34.56	2.496	.0303	.0421	390.4
19			7912	4680	2480	3275	2613	34.08	2.740	.0381	.0545	383.9
20	0.8	30,000	7917	1730	1858	2565	1532	39.99	2.342	0.0120	0.0149	409.3
21			7913	2200	2118	3055	2008	40.43	2.150	.0151	.0193	401.9
22			7912	2915	2394	3457	2422	39.90	2.192	.0203	.0270	390.2
23			7908	3770	2604	3744	2717	39.99	2.346	.0262	.0358	385.8
24			7905	4630	2773	4053	3011	40.04	2.459	.0321	.0450	380.5
25	1.0	30,000	7918	1749	1931	2937	1392	48.24	2.644	.0101	.0121	422.9
26			7915	2350	2398	3768	2227	48.28	2.132	.0135	.0170	405.0
27			7917	3110	2729	4311	2774	48.25	2.105	.0179	.0234	394.9
28			7913	4020	2978	4681	3154	48.07	2.219	.0232	.0312	387.4
29			7918	4920	3245	5063	3531	48.35	2.312	.0283	.0391	385.9
					CONFIGURATION B							
30	0.40	40,000	7905	1299	1158	1220	971	19.43	2.530	0.0186	0.0246	411.4
31			7918	1479	1338	1534	1268	19.52	2.222	.0210	.0293	399.5
32			7918	1858	1420	1630	1385	19.36	2.367	.0267	.0382	395.9
33			7903	2100	1460	1708	1451	19.65	2.453	.0297	.0428	398.1
34			7913	2365	1490	1721	1472	19.28	2.619	.0341	.0500	391.5
35	0.60	10,000	7919	2240	3308	4128	2624	72.11	2.114	.0086	.0106	404.8
36			7920	2710	3590	4589	3073	72.12	2.050	.0104	.0131	398.4
37			7919	3825	4040	5309	3811	72.10	2.064	.0147	.0192	392.4
38			7915	4840	4365	5774	4254	72.56	2.164	.0185	.0246	395.5
39			7922	6000	4670	6236	4768	71.05	2.238	.0235	.0322	388.0
40		20,000	7922	1891	2500	3176	2145	51.28	2.047	0.0102	0.0128	406.3
41			7913	2430	2727	3771	2741	51.33	1.881	.0132	.0168	394.2
42			7917	3215	3116	4131	3102	52.20	2.041	.0171	.0227	392.1
43			7908	4020	3346	4463	3431	51.92	2.147	.0215	.0293	390.0
44			7913	4890	3559	4728	3698	51.57	2.285	.0263	.0368	387.6
45		30,000	7914	1605	1861	2320	1670	34.51	2.075	0.0129	0.0166	402.2
46			7917	1941	2000	2559	1905	34.25	2.069	.0157	.0207	397.6
47			7919	2365	2164	2840	2169	34.44	2.088	.0191	.0258	394.5
48			7920	2765	2294	2996	2338	34.32	2.164	.0224	.0309	390.2
49			7921	3195	2410	3142	2482	34.44	2.258	.0258	.0362	390.5
50		40,000	7918	1579	1463	1810	1390	21.72	2.188	0.0202	0.0280	391.5
51			7911	1876	1520	1923	1498	21.86	2.267	.0238	.0334	390.9
52			7913	2175	1575	1958	1543	21.71	2.430	.0278	.0397	391.9
53			7912	2470	1624	2051	1637	21.67	2.501	.0317	.0458	389.1
54			7916	1319	1311	1602	1184	21.87	2.221	.0168	.0223	377.5
55			7884	1576	1442	1819	1387	22.05	2.176	.0199	.0272	388.5
56			7889	1842	1531	1916	1499	21.74	2.250	.0235	.0332	387.2
57			7892	2150	1572	2004	1578	22.03	2.359	.0269	.0380	390.2
58			7859	2455	1624	2079	1662	22.07	2.454	.0309	.0444	383.5
59		45,000	7913	1443	1165	1416	1081	16.97	2.413	0.0236	0.0330	403.4
60			7913	1626	1210	1473	1134	16.88	2.501	.0268	.0380	398.5
61			7923	1846	1260	1519	1187	16.92	2.617	.0303	.0437	399.3
62			7908	2085	1275	1557	1229	17.00	2.734	.0341	.0493	395.4
63	0.80	40,000	----	1395	1451	1975	1327	25.58	2.145	0.0151	0.0198	363.6
64			7917	1659	1594	2182	1539	25.69	2.114	.0179	.0241	394.6
65			7913	2355	1774	2449	1806	25.55	2.286	.0256	.0359	389.8
66			7914	2700	1861	2541	1903	25.46	2.397	.0295	.0422	388.3
67			7913	1454	1474	2001	1354	25.60	2.162	.0158	.0207	405.5
68			7914	1756	1609	2240	1586	25.71	2.122	.0190	.0256	400.1
69			7913	2050	1708	2360	1713	25.50	2.194	.0223	.0309	396.1
70			7914	2370	1792	2457	1821	25.69	2.286	.0256	.0360	394.3
71			7910	2740	1873	2566	1917	25.71	2.406	.0296	.0423	396.6
72	1.0	40,000	7913	1507	1651	2497	1528	30.86	2.067	0.0136	0.0174	409.2
73			7913	1843	1784	2706	1738	30.85	2.087	.0166	.0218	406.1
74			7916	2200	1946	2948	1979	30.81	2.095	.0198	.0268	401.0
75			7913	2570	2054	3091	2123	30.58	2.178	.0233	.0323	399.7
76			7926	3005	2134	3270	2297	31.02	2.263	.0269	.0380	395.9

DATA WITH AFTERBURNING

Afterburner outlet total temperature T_8 (°R)	Afterburner combustion efficiency η_t	Engine-inlet total pressure P_1 (lb/sq ft)	Turbine-outlet total pressure P_5 (lb/sq ft)	Afterburner inlet static pressure p_6 (lb/sq ft)	Afterburner outlet total pressure P_8 (lb/sq ft)	Exhaust static pressure p_0 (lb/sq ft)	Engine-inlet total temperature T_1 (°R)	Turbine outlet total temperature T_5 (°R)	Run
CONFIGURATION A									
1898	0.443	696.0	1220	1117	1156	616.4	426	1452	1
2452	.661	694.3	1369	1265	1290	617.9	427	1580	2
2666	.652	697.6	1416	1318	1337	617.0	427	1651	3
2717	.590	696.2	1458	1354	1372	618.4	427	1695	4
2736	.499	698.3	1445	1341	1359	620.1	427	1711	5
1850	0.584	1854	2847	2562	2665	1437	526	1448	6
2291	.762	1853	3136	2861	2936	1449	522	1578	7
2606	.808	1852	3320	3050	3112	1450	522	1674	8
2879	.810	1856	3485	3216	3264	1448	521	1759	9
1556	0.343	1237	1852	1647	1734	962.0	478	1336	10
1842	.514	1238	2015	1818	1889	962.4	479	1440	11
2328	.708	1234	2234	2047	2095	965.9	481	1584	12
2647	.745	1236	2358	2170	2209	965.9	480	1669	13
2869	.700	1236	2459	2275	2305	965.2	482	1751	14
1690	0.333	793.1	1313	1183	1231	611.2	441	1418	15
2219	.653	799.7	1445	1321	1358	617.5	444	1537	16
2625	.690	796.0	1588	1463	1486	620.8	444	1664	17
2794	.625	796.9	1652	1535	1552	617.0	443	1734	18
3010	.588	799.0	1704	1586	1599	620.4	441	1774	19
1661	0.365	950.4	1481	1324	1382	615.1	467	1377	20
2034	.572	949.0	1644	1495	1539	613.7	467	1506	21
2453	.682	951.8	1784	1637	1668	615.8	466	1620	22
2715	.670	951.6	1883	1740	1763	620.8	465	1695	23
2985	.681	954.6	1978	1837	1856	615.5	463	1754	24
1378	0.151	1180	1631	1428	1513	613.8	494	1277	25
1938	.552	1182	1915	1736	1790	619.3	493	1472	26
2341	.692	1182	2099	1917	1984	620.8	492	1595	27
2650	.714	1183	2226	2049	2084	627.2	490	1679	28
2918	.723	1184	2347	2173	2197	625.9	488	1760	29
CONFIGURATION B									
1900	0.307	432.4	791.1	710.9	735.9	384.9	408	1512	30
2490	.629	433.8	889.4	809.3	829.1	380.6	407	1665	31
2716	.611	428.9	923.3	843.9	859.3	383.3	407	1735	32
2812	.608	436.3	952.9	873.5	886.4	387.1	408	1780	33
2908	.569	432.8	957.5	879.4	888.6	384.9	410	1788	34
1766	0.604	1852	2801	2499	2613	1443	522	1425	35
1995	.743	1853	2961	2659	2758	1441	521	1488	36
2382	.850	1850	3207	2900	2984	1447	521	1596	37
2602	.834	1860	3356	3053	3122	1446	523	1679	38
2968	.881	1847	3503	3199	3263	1447	521	1761	39
1835	0.601	1231	2012	1801	1877	959.4	480	1447	40
2117	.715	1236	2151	1942	2004	964.8	480	1508	41
2452	.797	1234	2343	2130	2180	965.3	466	1614	42
2721	.806	1245	2456	2243	2284	966.0	469	1696	43
2954	.783	1244	2545	2330	2366	967.2	474	1762	44
1979	0.590	794.7	1403	1260	1304	627.1	440	1486	45
2243	.690	788.2	1478	1335	1372	618.4	441	1565	46
2519	.755	793.6	1563	1423	1454	616.1	441	1643	47
2719	.763	792.4	1623	1487	1511	620.8	439	1701	48
2877	.752	796.9	1673	1533	1556	624.8	442	1748	49
2502	0.663	492.4	989.2	899.8	920.6	380.1	424	1635	50
2677	.678	496.5	1030	937.2	956.8	381.9	424	1689	51
2795	.638	491.0	1039	952.9	974.6	381.4	424	1730	52
2926	.627	491.7	1072	985.0	996.7	382.6	425	1777	53
2120	.523	493.3	324.2	849.3	859.9	382.3	420	1478	54
2445	.649	496.7	990	915.2	924.1	380.0	420	1622	55
2668	.670	488.4	1026	945.0	952.5	377.7	419	1694	56
2774	.661	497.6	1057	980.1	984.6	383.4	418	1730	57
2904	.642	496.9	1087	1010	1011	387.2	420	1763	58
2477	0.547	386.1	774.2	703.7	719.0	295.0	426	1678	59
2609	.547	385.6	789.6	721.3	734.9	292.7	426	1718	60
2723	.537	386.6	812.1	742.0	754.3	298.0	424	1752	61
2754	.502	383.3	823.1	759.7	765.4	296.5	422	1771	62
2048	0.537	590.8	1063	957.8	988.0	380.0	438	1378	63
2352	.665	592.2	1130	1024	1051	384.9	439	1588	64
2754	.680	590.5	1222	1117	1133	383.5	440	1715	65
2900	.659	588.0	1256	1145	1161	383.0	442	1758	66
2104	.560	591.2	1067	962	989.4	381.4	441	1537	67
2429	.686	597.2	1147	1037	1066	383.0	440	1626	68
2621	.694	587.3	1181	1077	1098	377.1	437	1682	69
2762	.683	594.3	1219	1119	1138	384.7	438	1724	70
2901	.661	596.5	1260	1151	1168	385.2	437	1783	71
1999	0.565	735.6	1246	1122	1158	380.4	470	1510	72
2244	.642	739.1	1321	1193	1225	383.2	471	1591	73
2533	.725	734.9	1397	1273	1299	380.8	469	1674	74
2743	.733	736.3	1445	1321	1343	380.4	472	1742	75
2901	.723	744.0	1511	1384	1404	386.3	468	1781	76

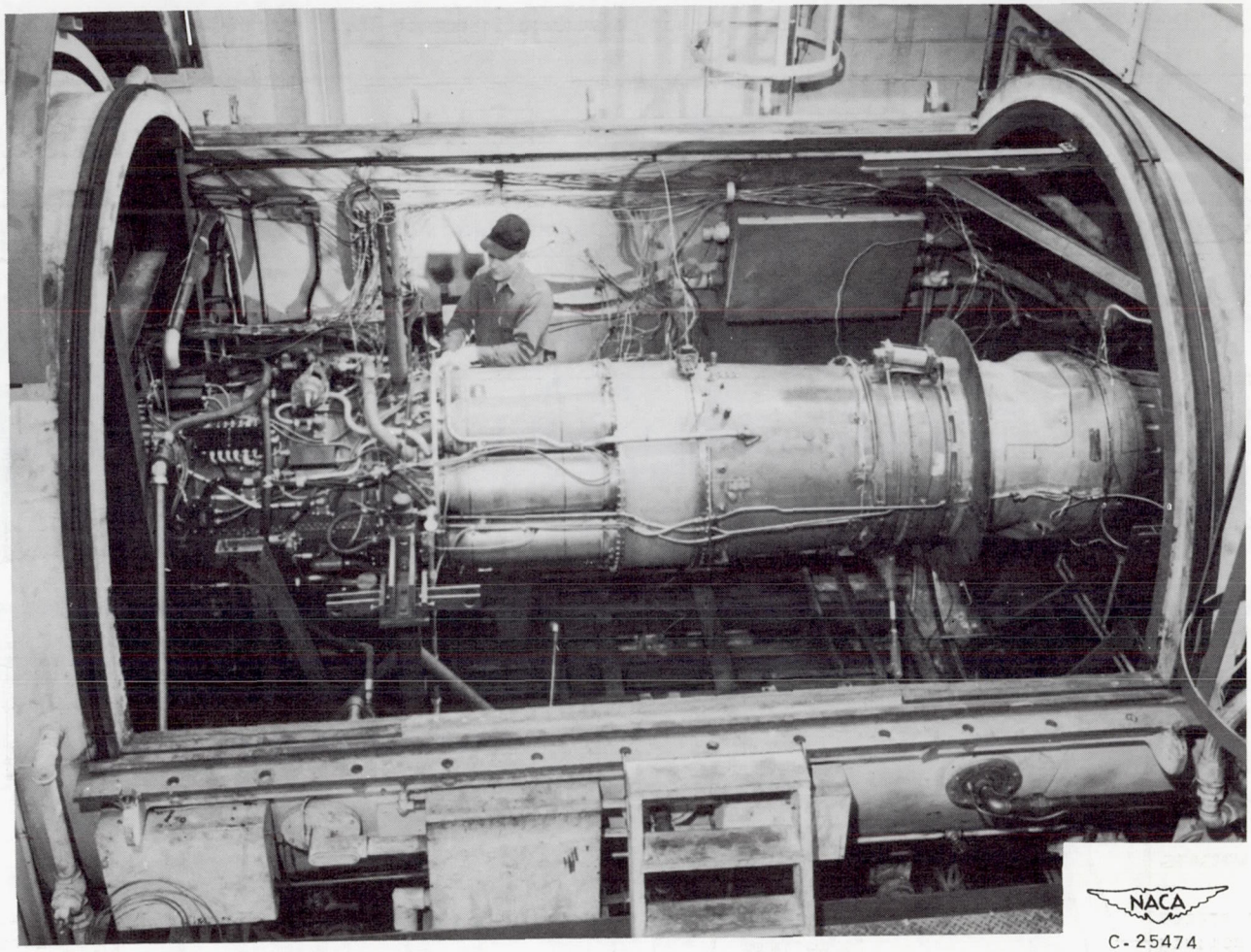

(a) Photograph of installation.

Figure 1. - Engine and afterburner installation in altitude chamber.

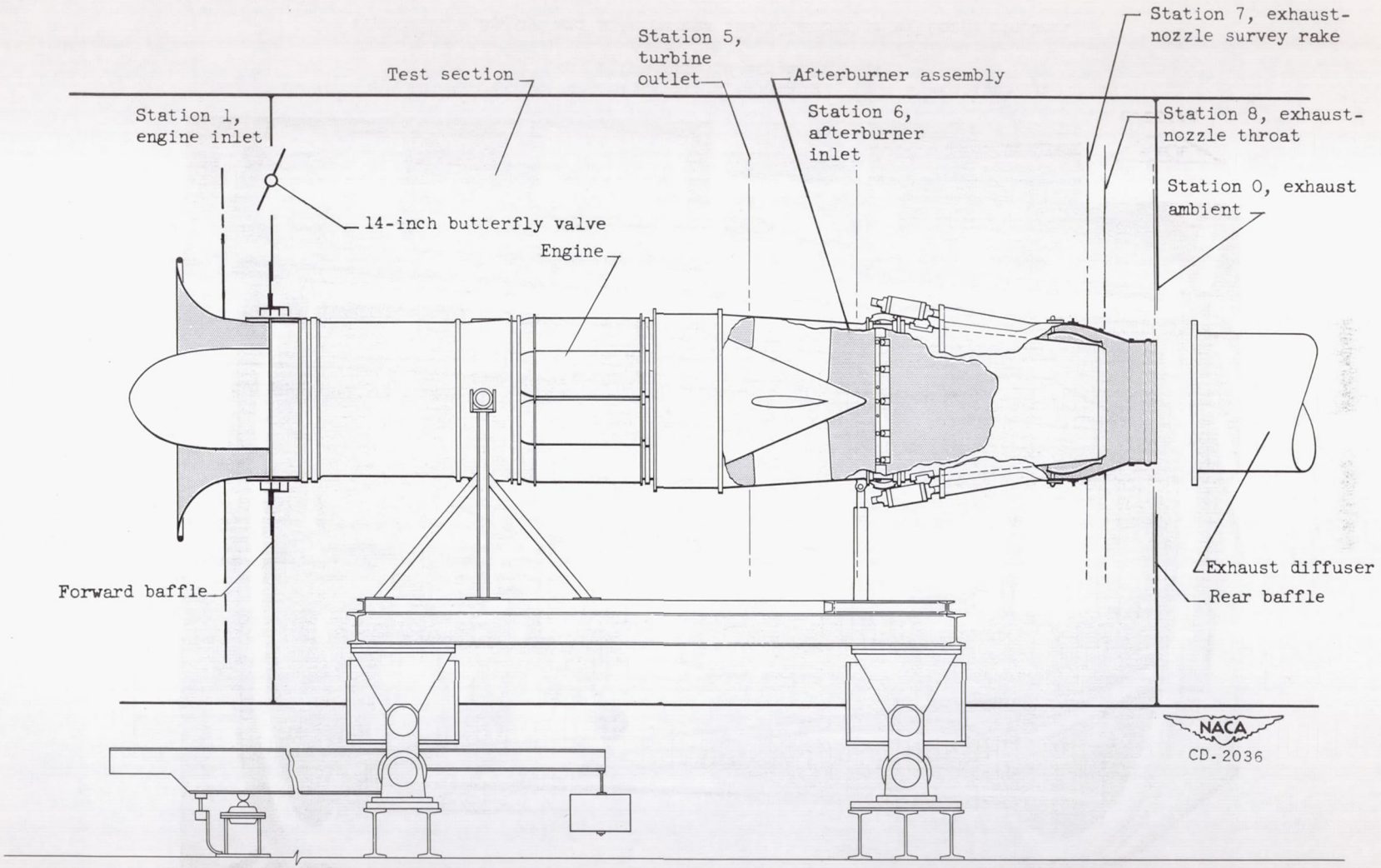

(b) Schematic diagram of installation.

Figure 1. - Concluded. Engine and afterburner installation in altitude chamber.

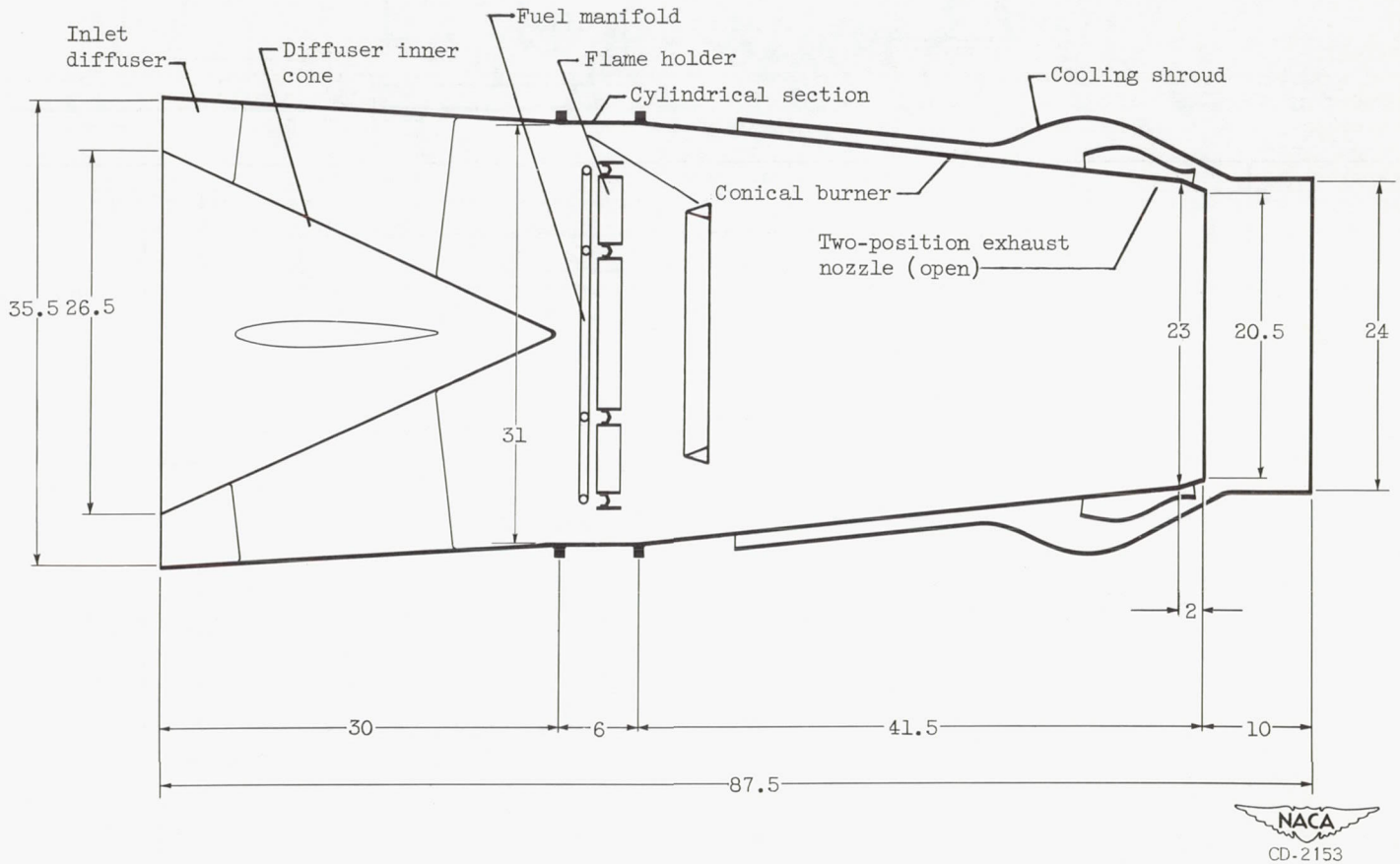

Figure 2. - Inlet diffuser and afterburner assembly. (All dimensions in inches.)

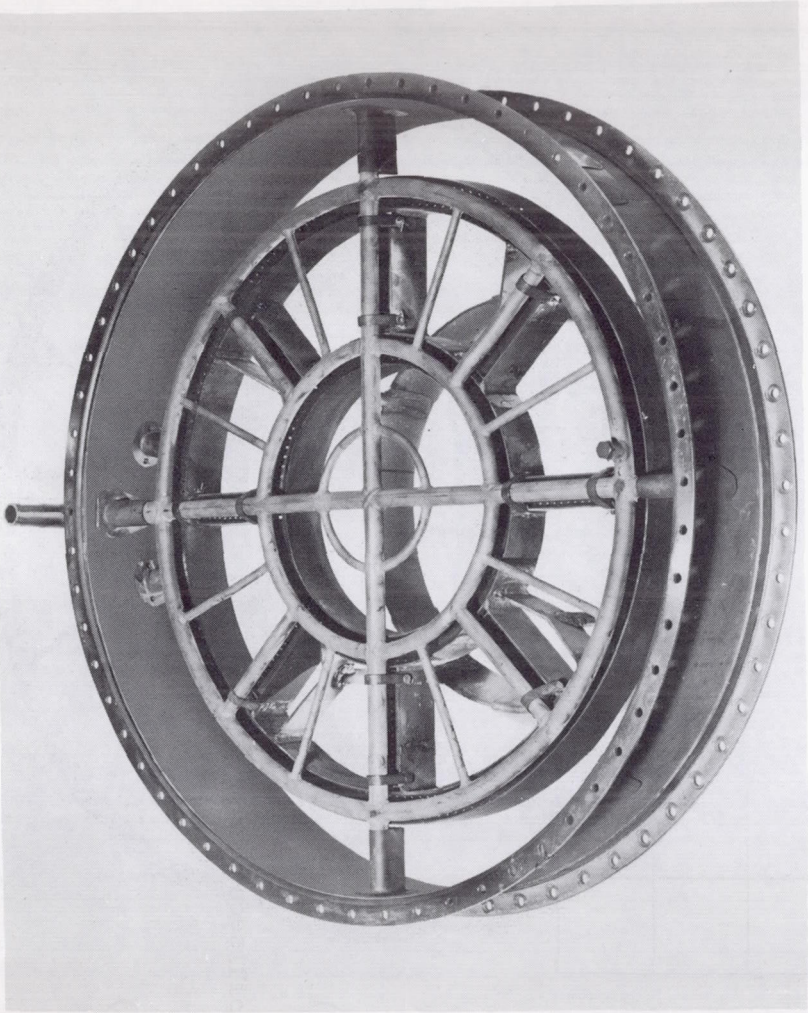

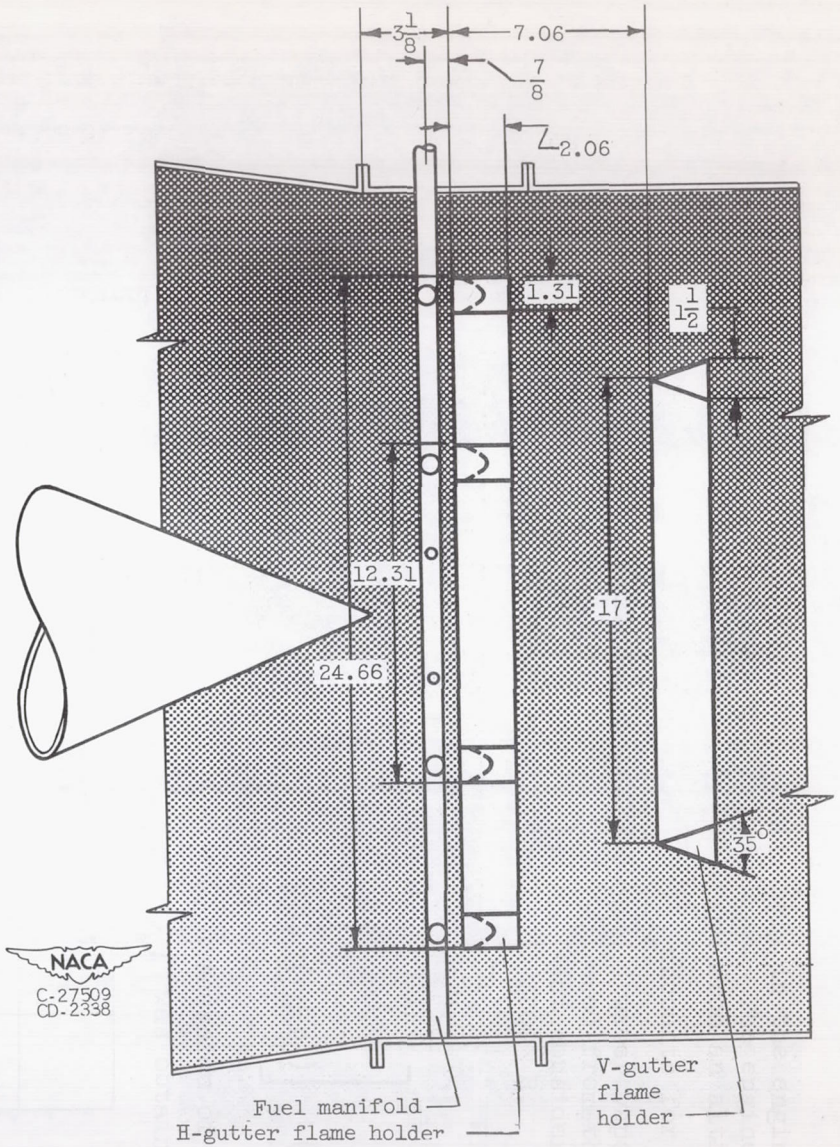

(a) Configuration A.

Figure 3. - Installation of fuel-system and flame-holder configurations. (All dimensions in inches.)

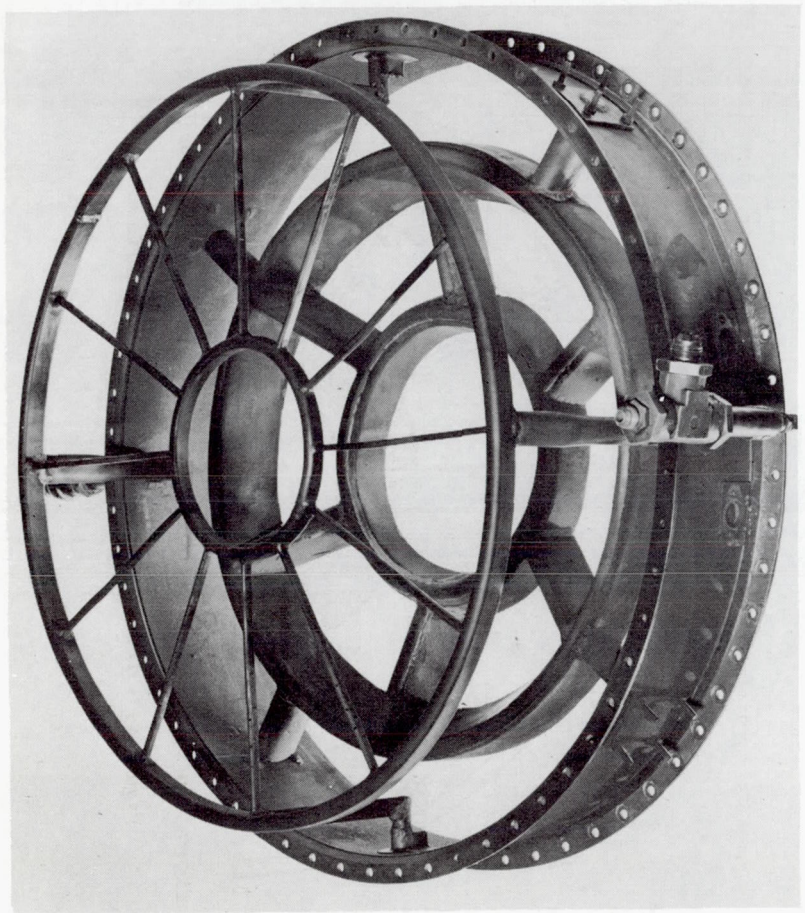

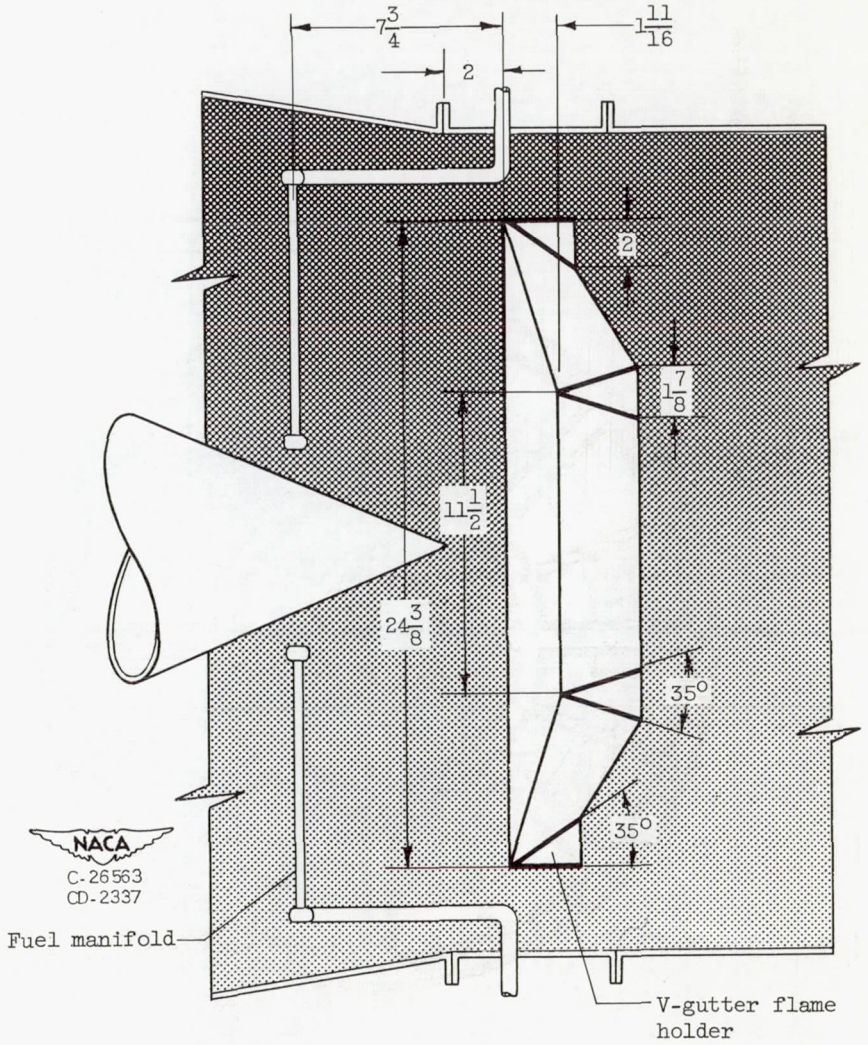

(b) Configuration B.

Figure 3. - Concluded. Installation of fuel-system and flame-holder configurations. (All dimensions in inches.)

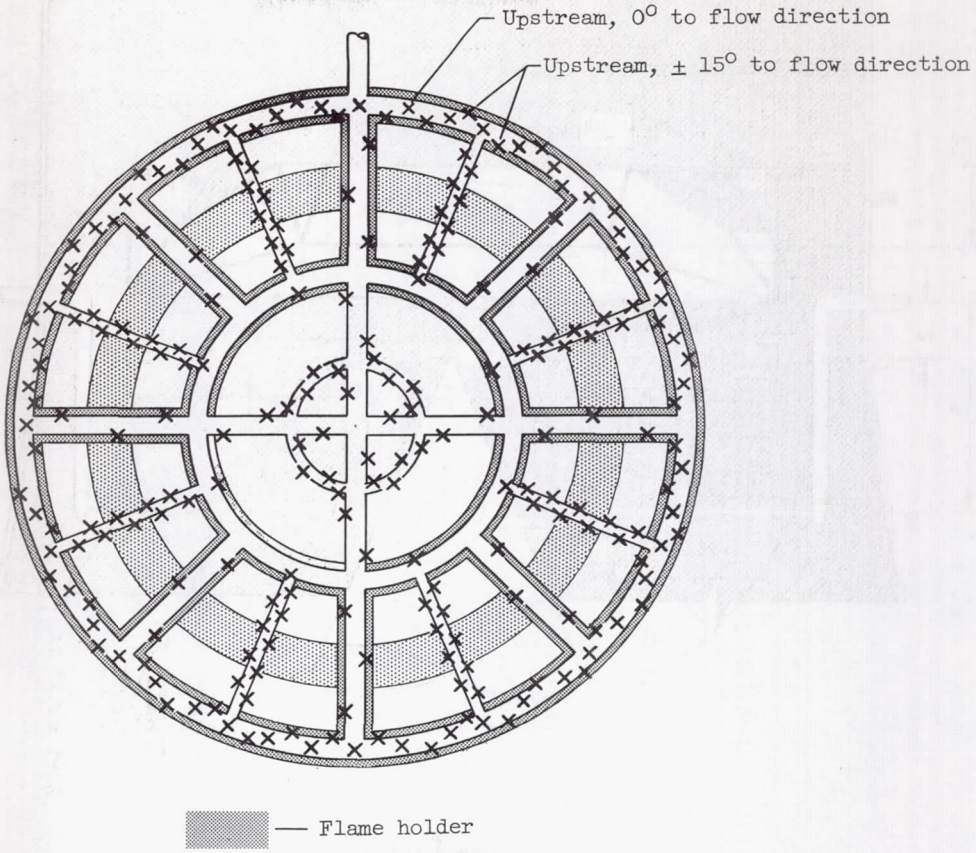

(a) Configuration A; diameter of orifices, 0.025 inch; number of orifices, 226.

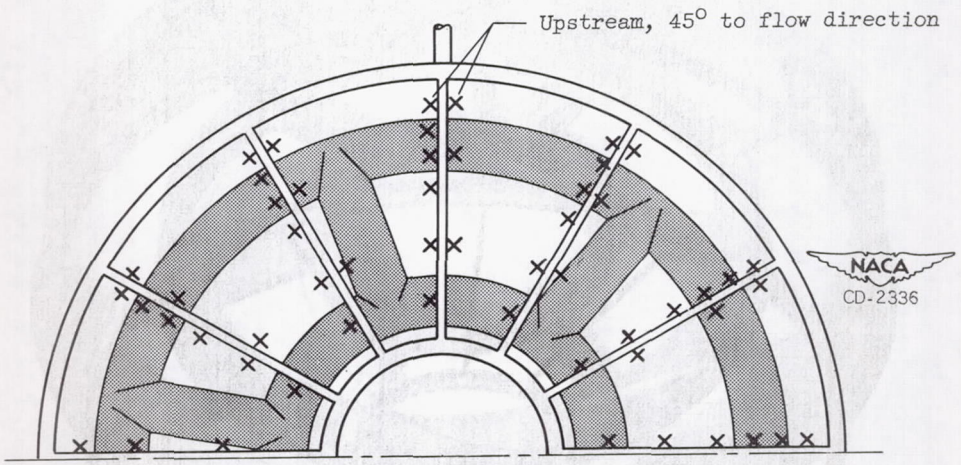

(b) Configuration B; diameter of orifices, 0.030 inch; number of orifices, 108.

Figure 4. - Location of fuel orifices in manifolds.

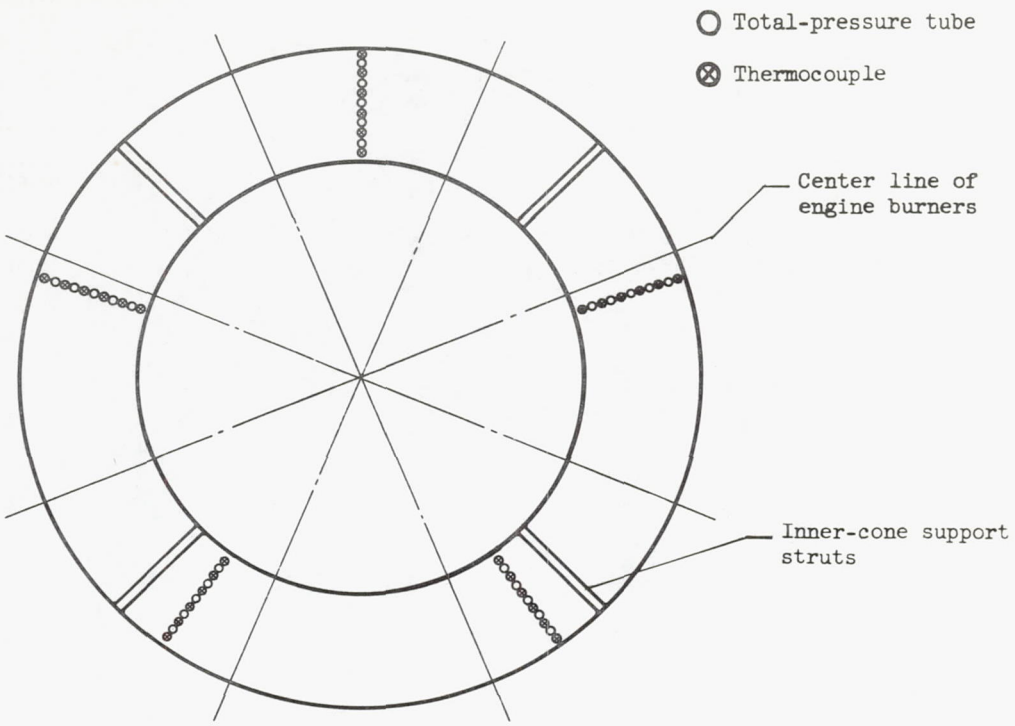

(a) Turbine outlet (diffuser inlet), station 5, $4\frac{1}{2}$ inches downstream of turbine flange.

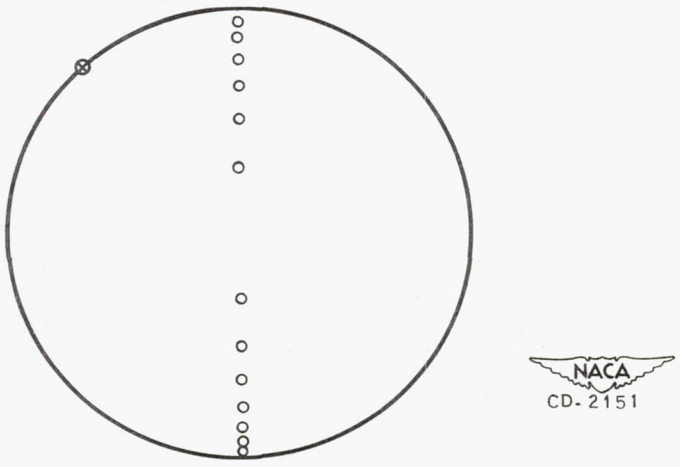

(b) Exhaust-nozzle inlet, station 7, 5 inches upstream of outlet.

Figure 5. - Location of pressure and temperature instrumentation installed in the afterburner; looking downstream.

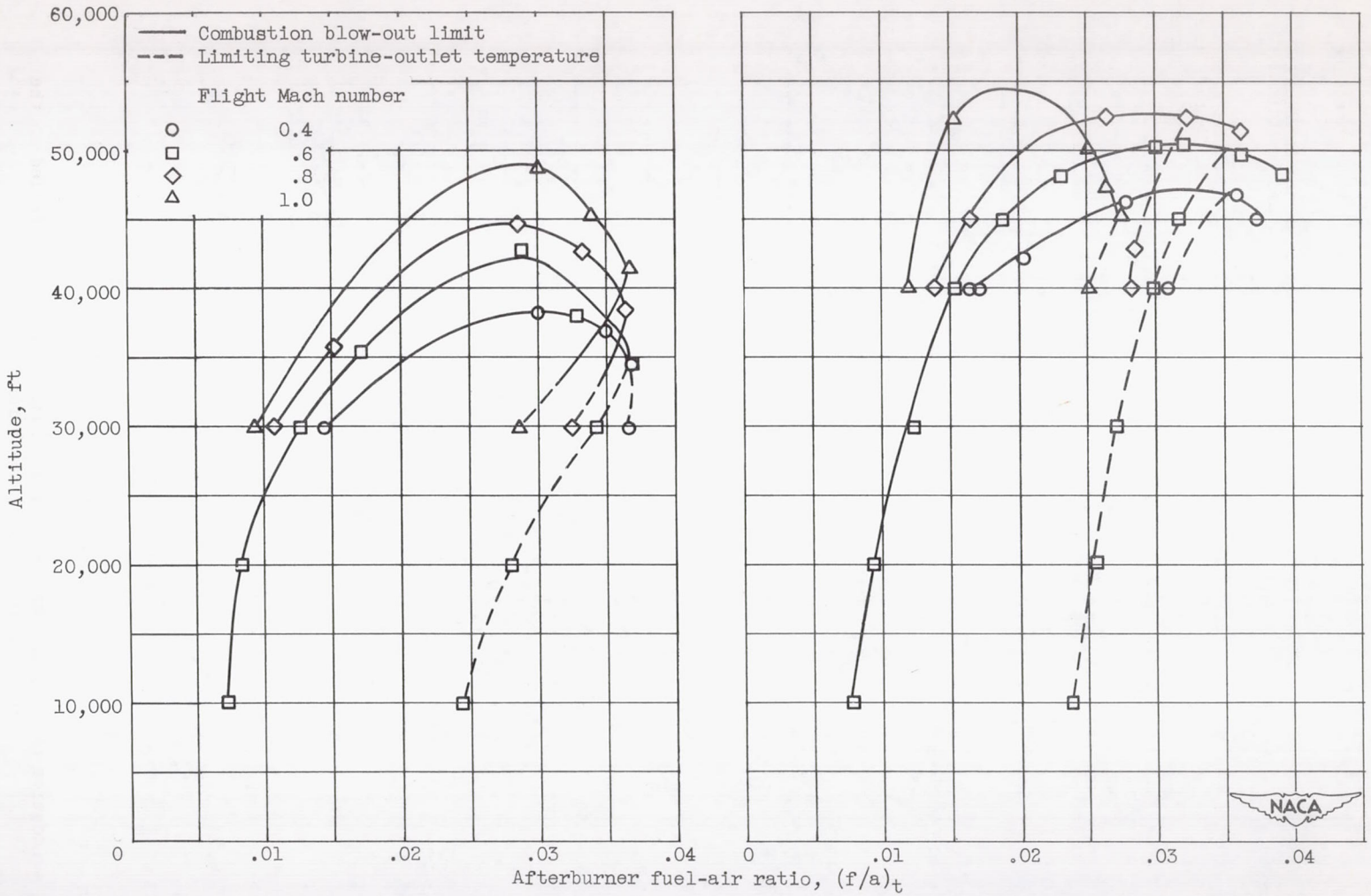

(a) Configuration A.

(b) Configuration B.

Figure 6. - Operable range of afterburner configurations at several flight Mach numbers.

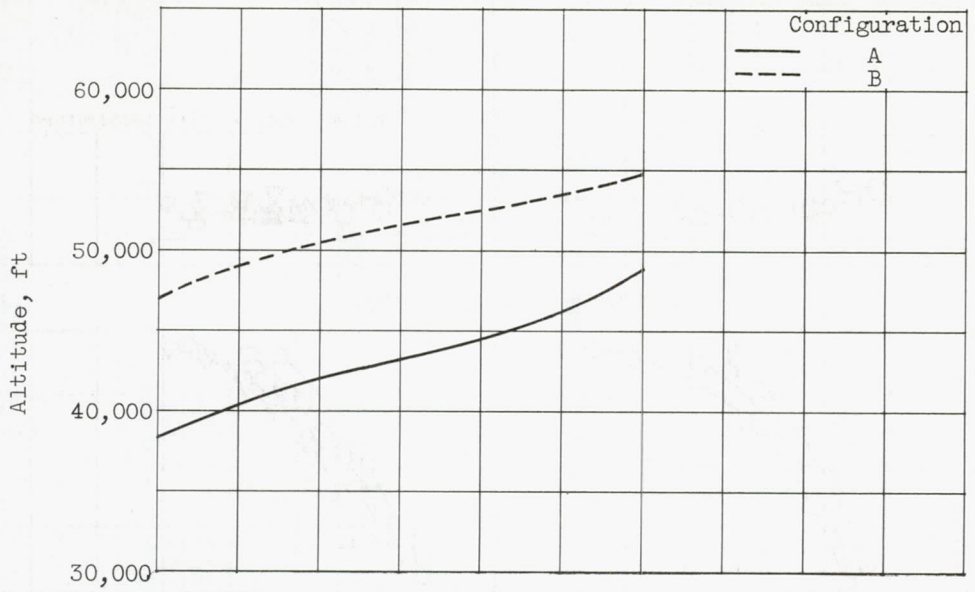

(a) Effect of flight Mach number on altitude limit.

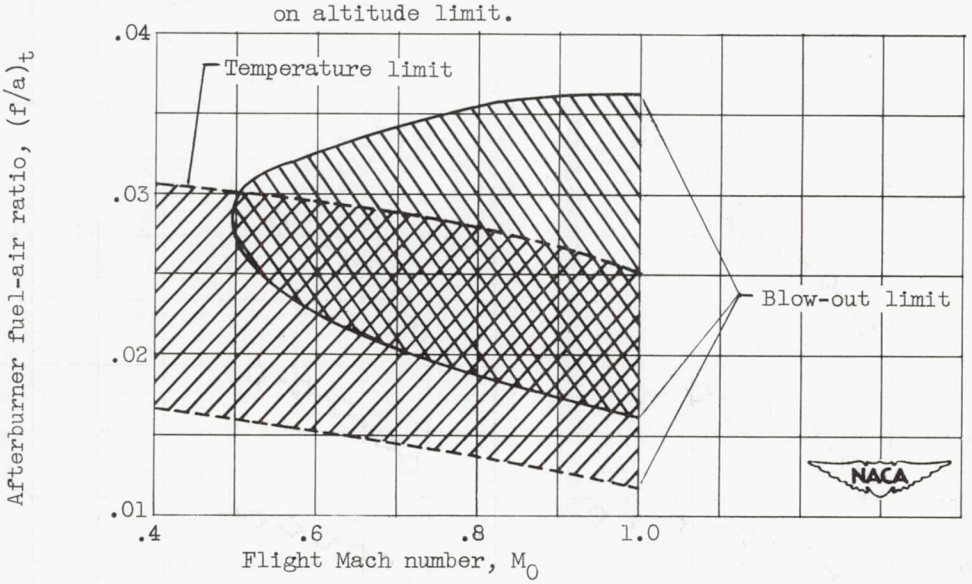

(b) Effect of flight Mach number on afterburner fuel-air ratio at altitude of 40,000 feet.

Figure 7. - Effect of flight Mach number on operational limits.

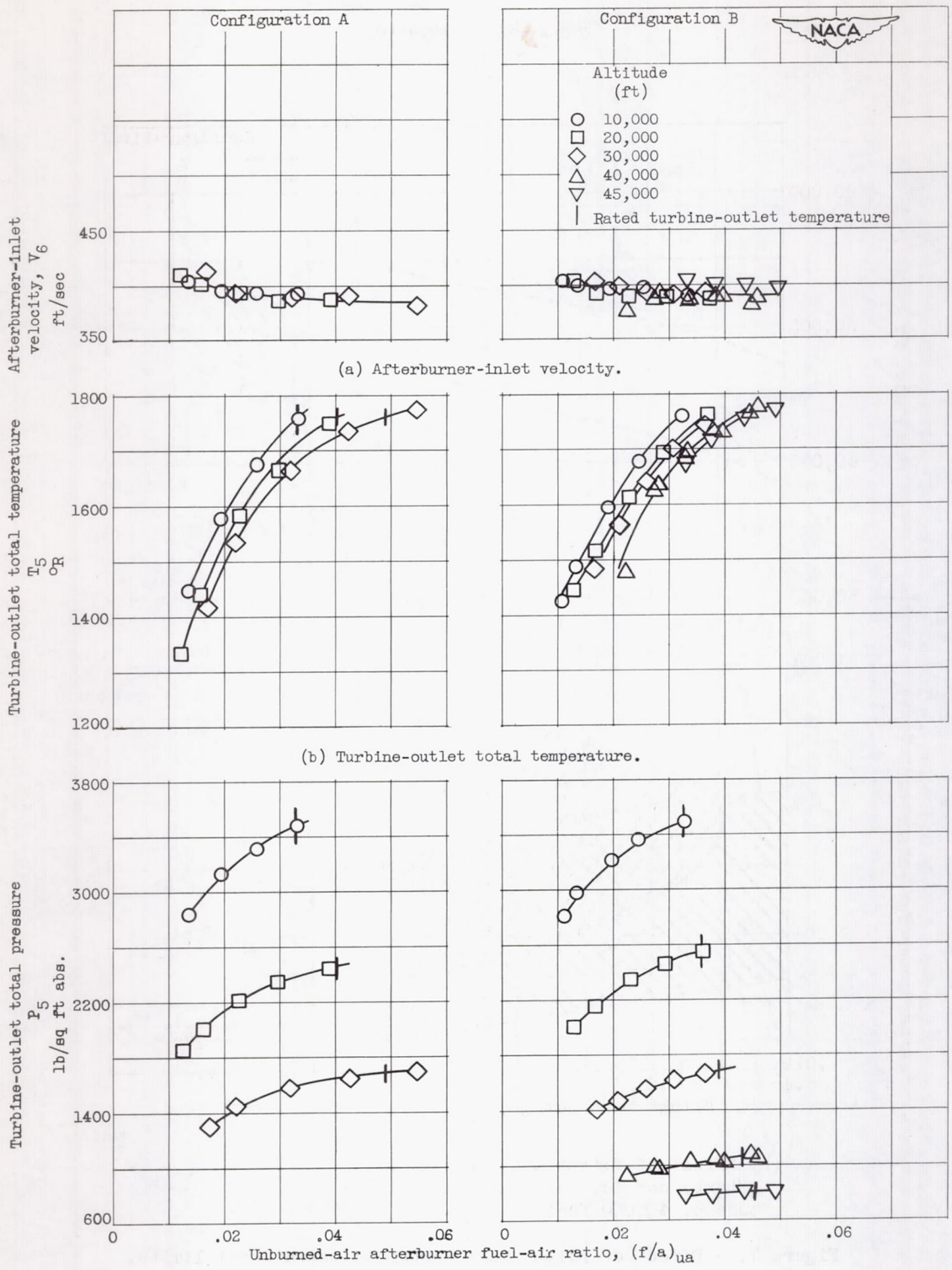

Figure 8. - Variation of afterburner inlet conditions with fuel-air ratio at several altitudes. Flight Mach number, 0.6.

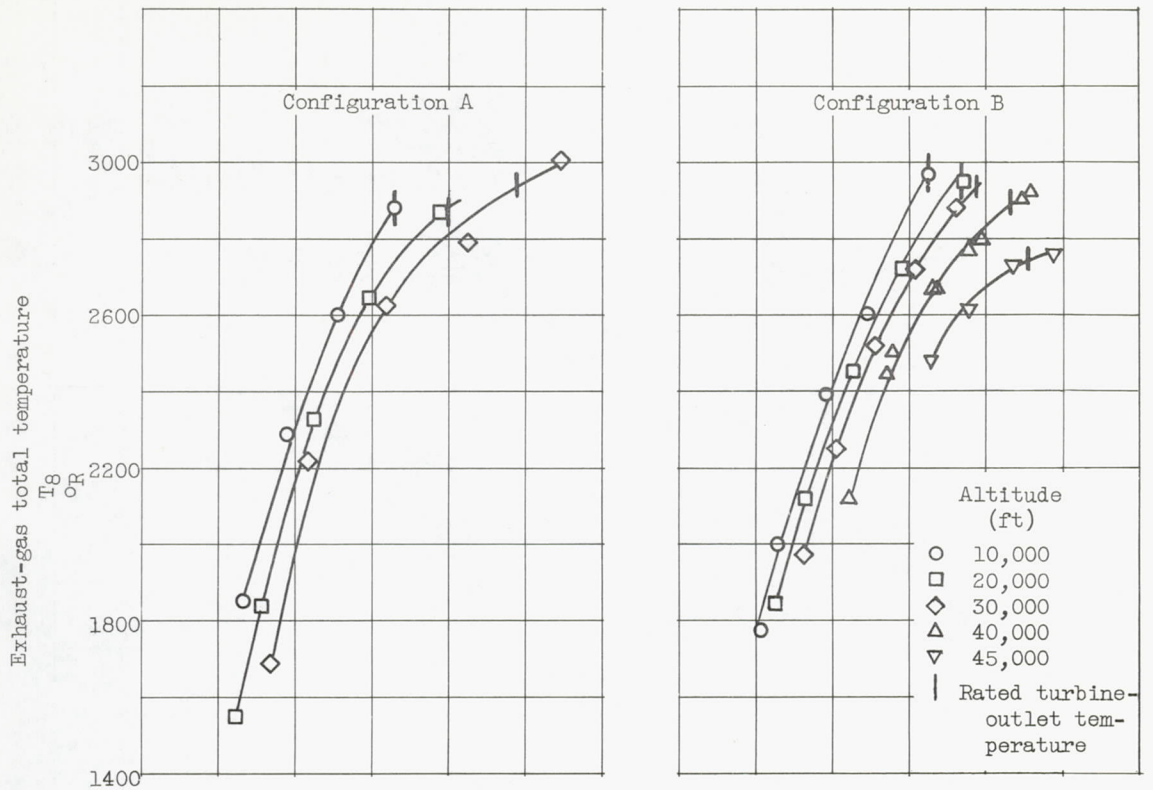

(a) Exhaust-gas total temperature.

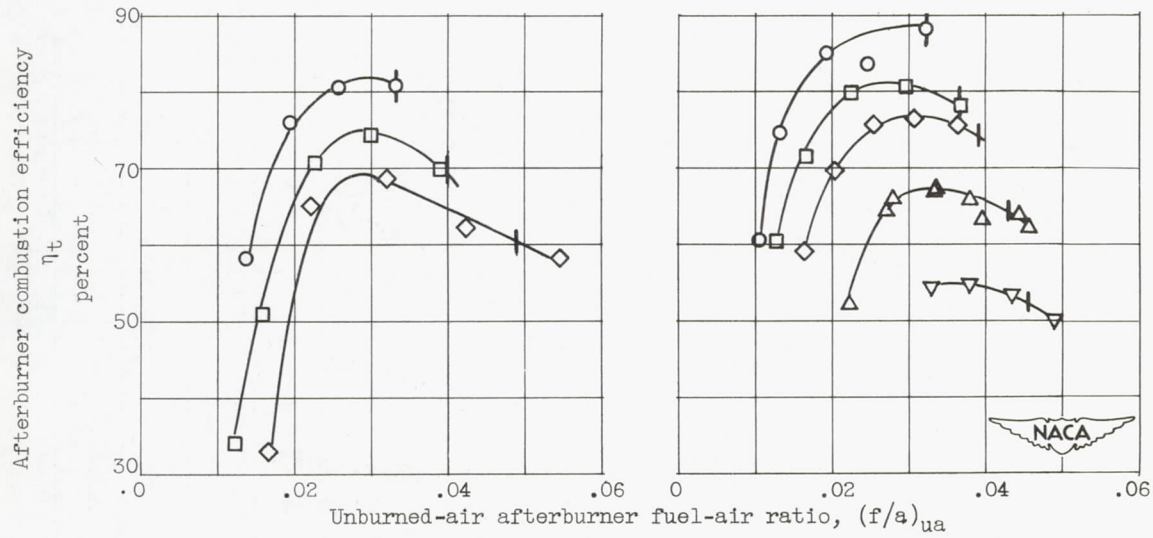

(b) Afterburner combustion efficiency.

Figure 9. - Variation of exhaust-gas total temperature and afterburner combustion efficiency with fuel-air ratio at several altitudes. Flight Mach number, 0.6.

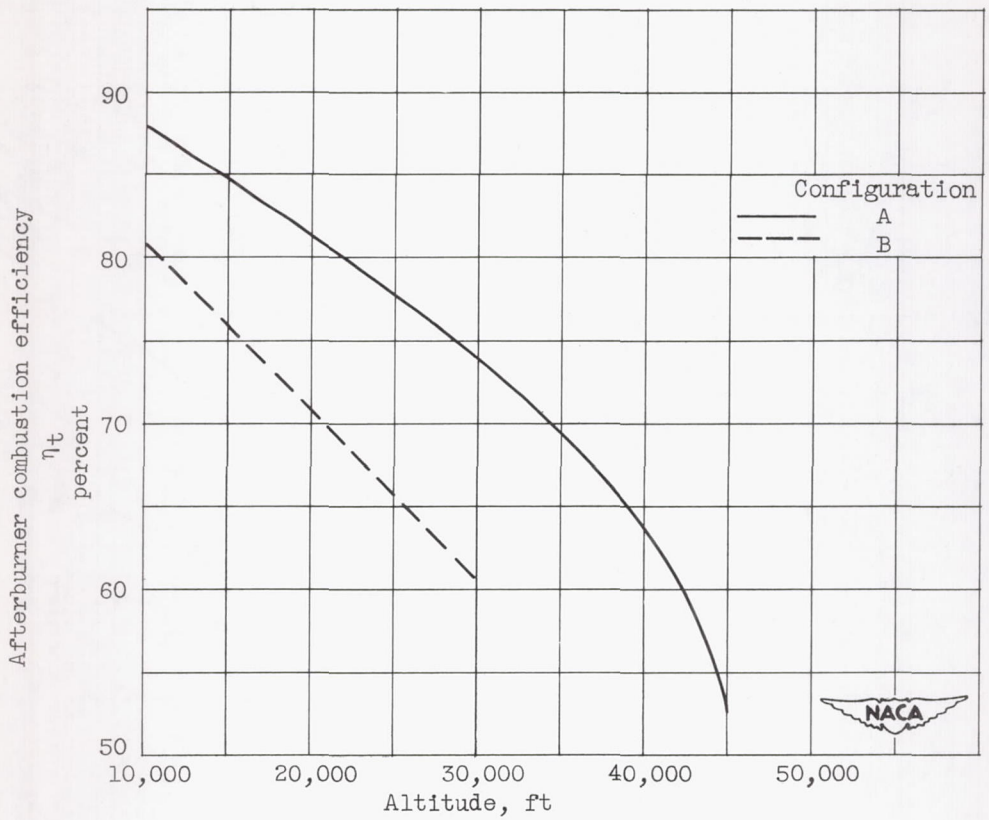

Figure 10. - Effect of altitude on combustion efficiency at rated turbine-outlet temperature. Flight Mach number, 0.6.

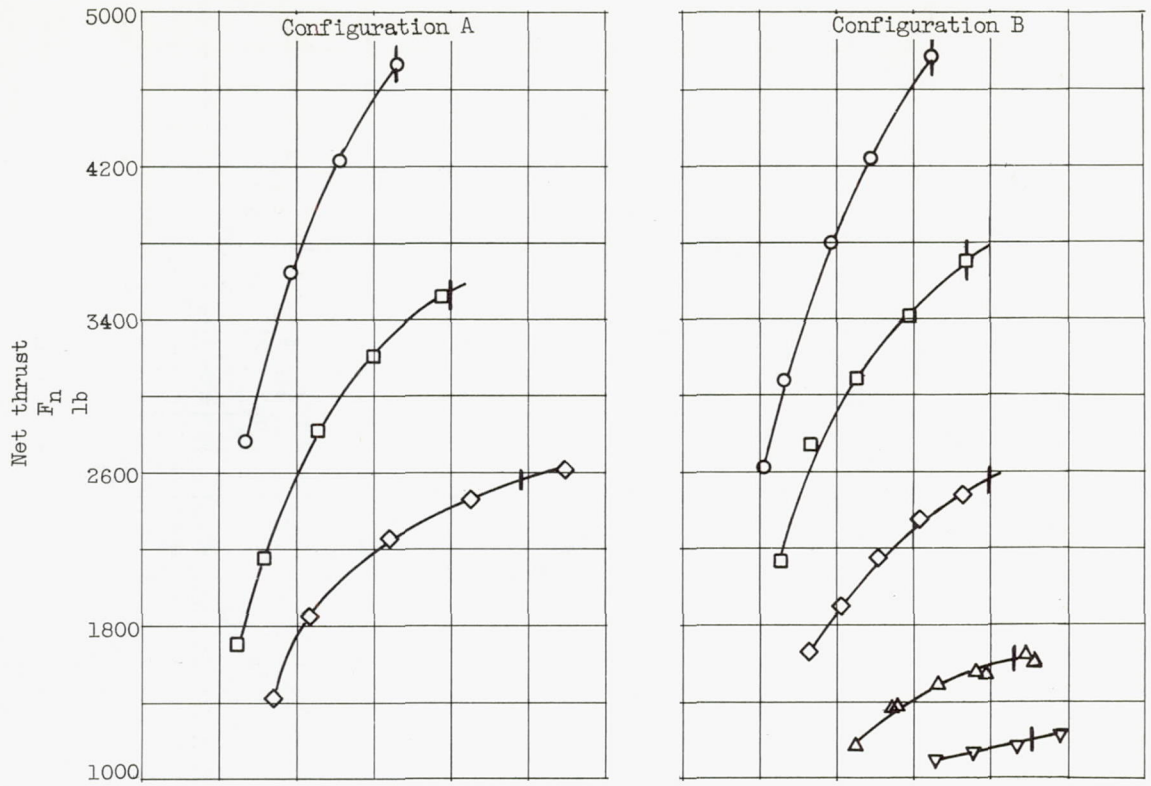

(a) Net thrust.

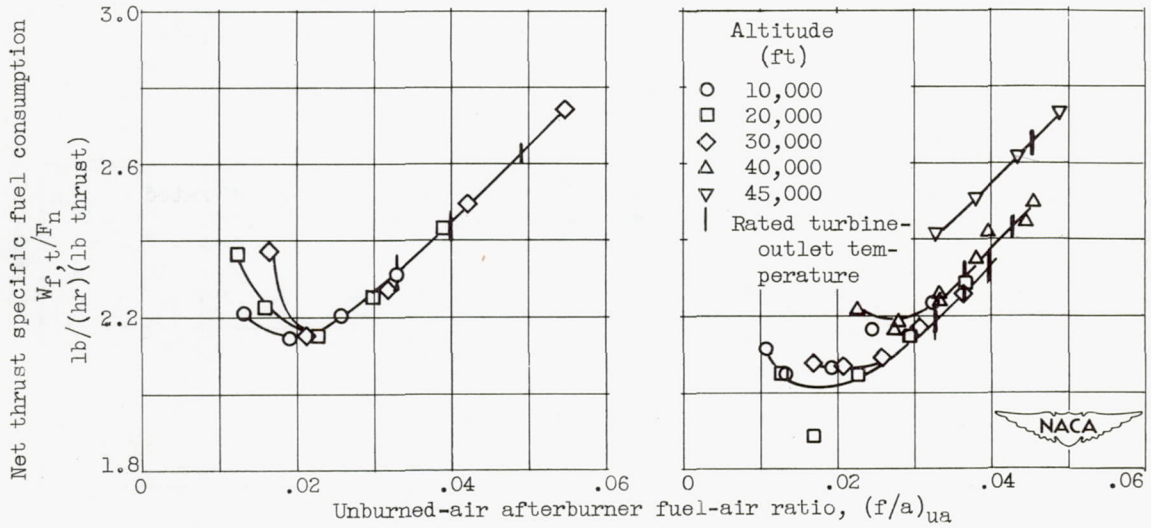

(b) Net thrust specific fuel consumption.

Figure 11. - Variation of over-all afterburner performance with afterburner fuel-air ratio at several altitudes. Flight Mach number, 0.6.

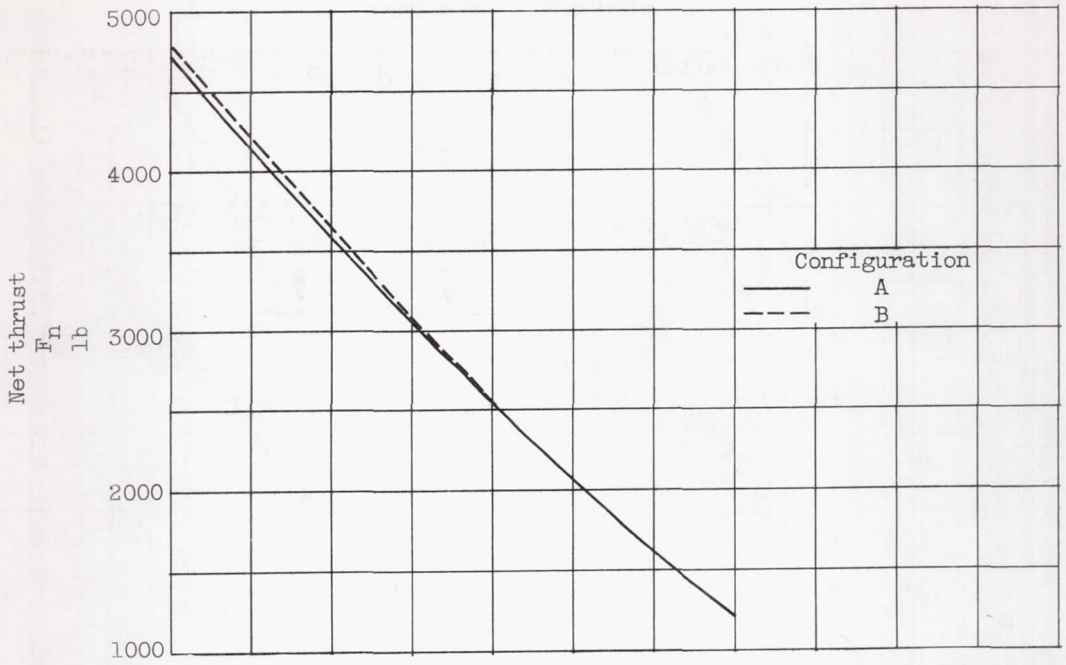

(a) Net thrust.

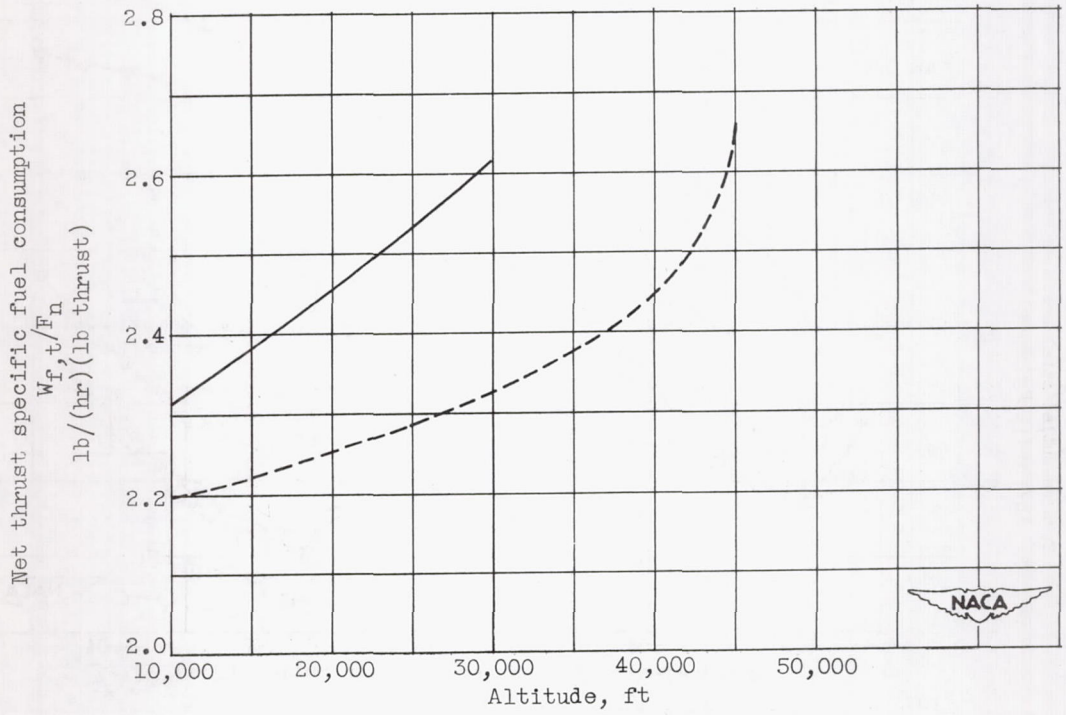

(b) Specific fuel consumption.

Figure 12. - Variation of over-all afterburner performance with altitude at rated turbine-outlet total temperature. Flight Mach number, 0.6.

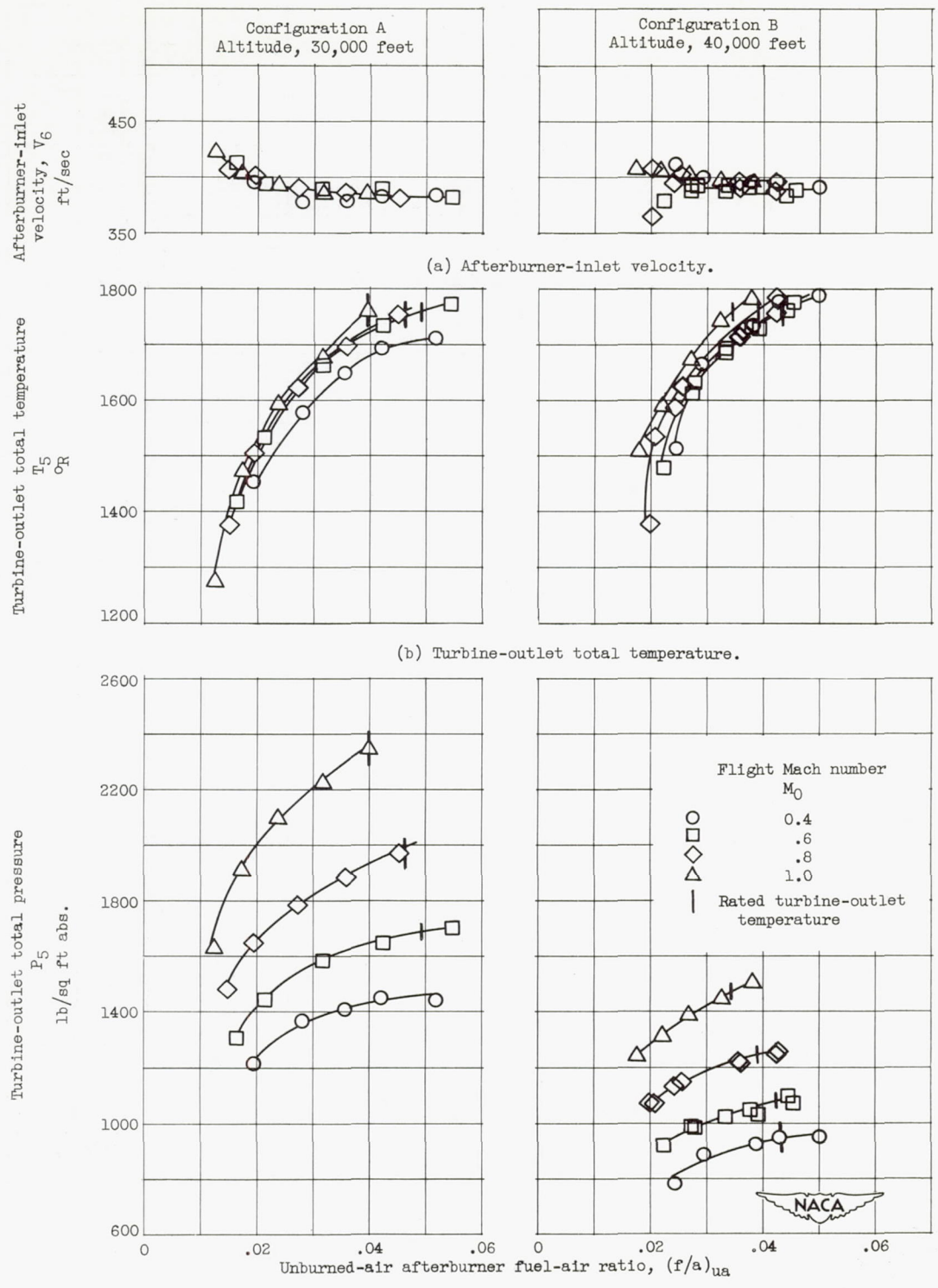

Figure 13. - Variation of afterburner inlet conditions with afterburner fuel-air ratio at several flight Mach numbers.

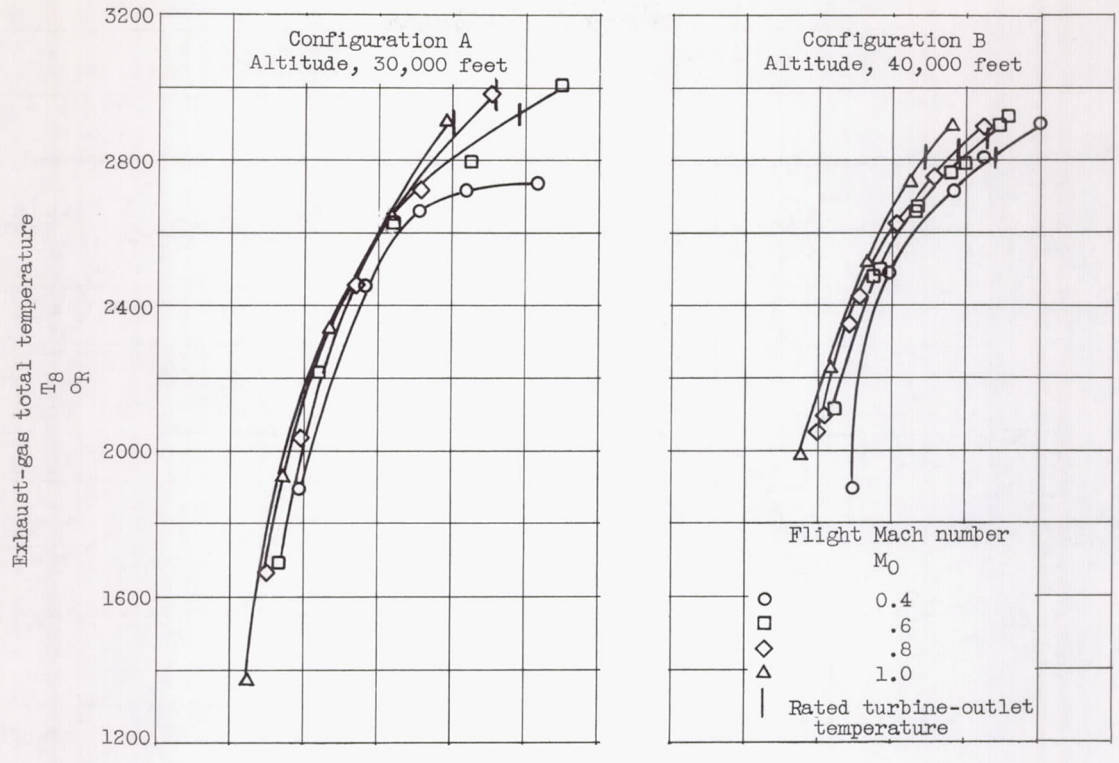

(a) Exhaust-gas total temperature.

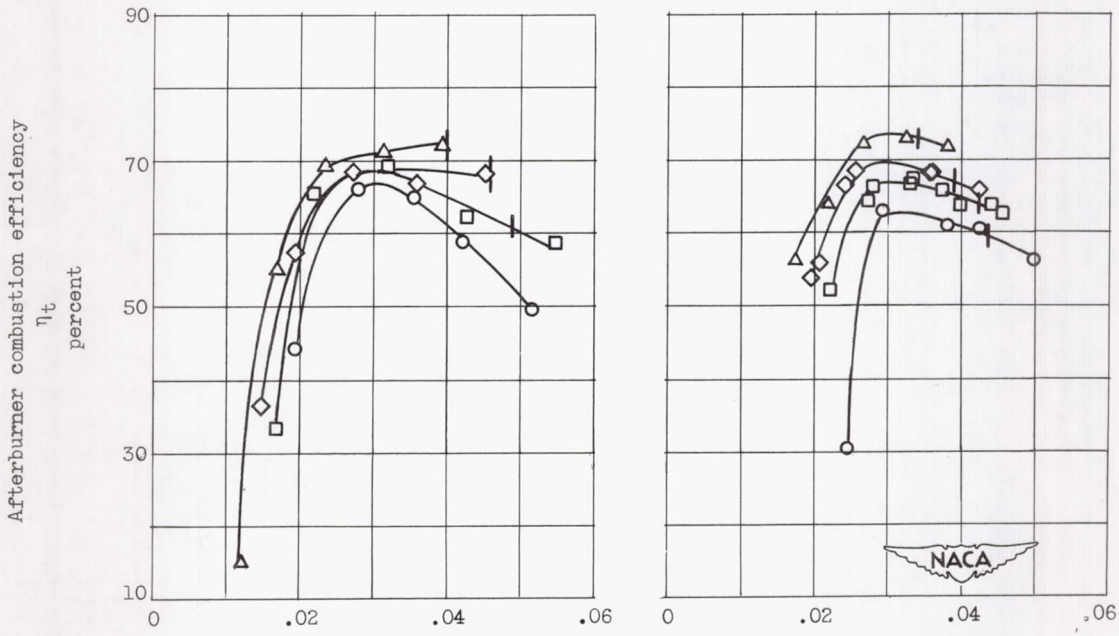

(b) Afterburner combustion efficiency.

Figure 14. - Variation of exhaust-gas total temperature and afterburner combustion efficiency with afterburner fuel-air ratio at several flight Mach numbers.

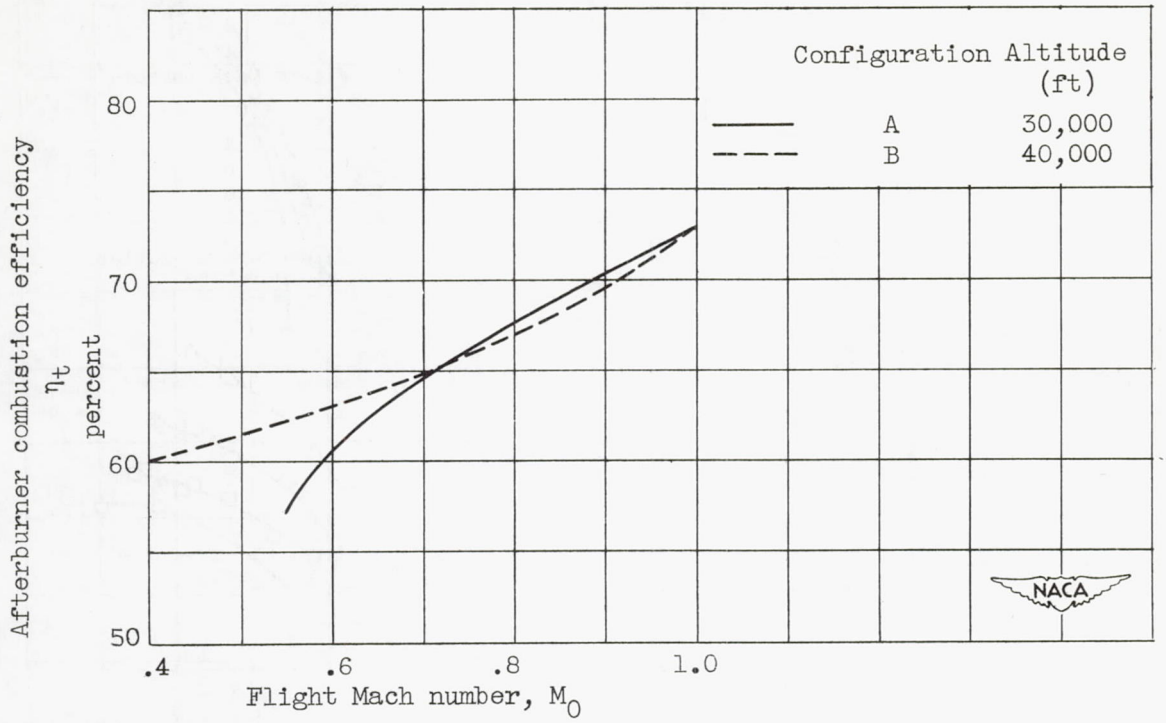

Figure 15. - Effect of flight Mach number on afterburner combustion efficiency. (Cross plot of fig. 14(b).)

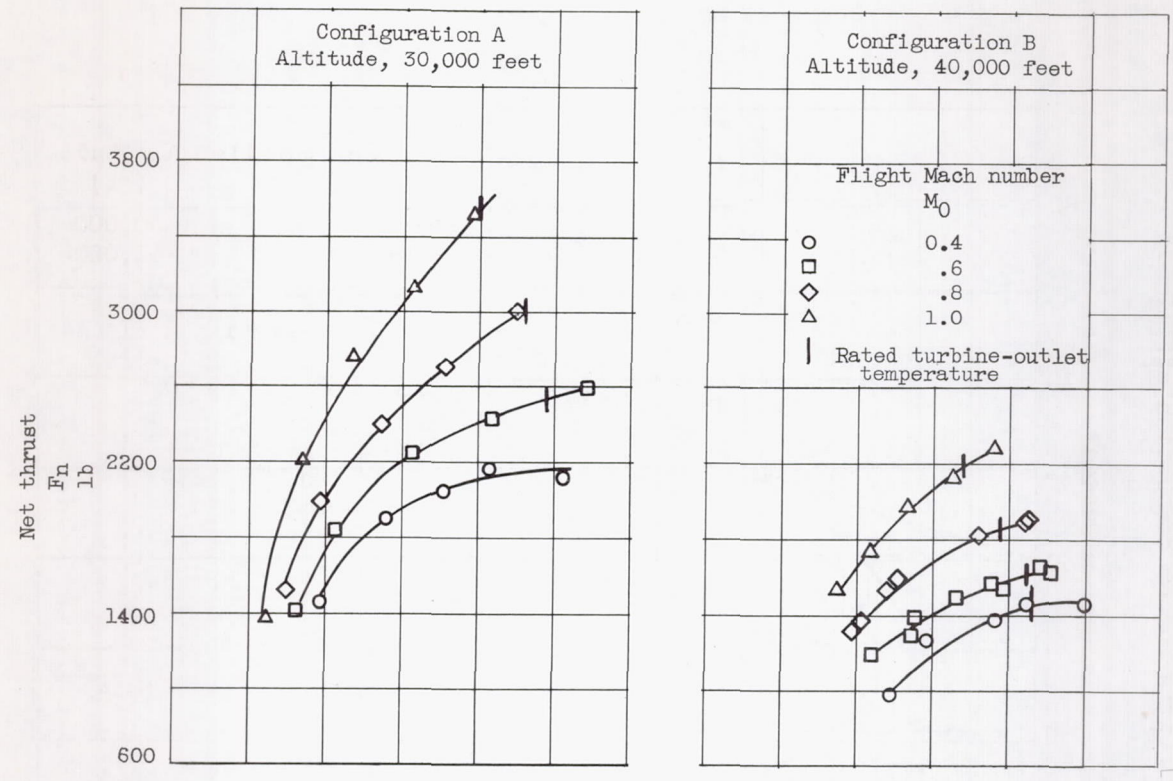

(a) Net thrust.

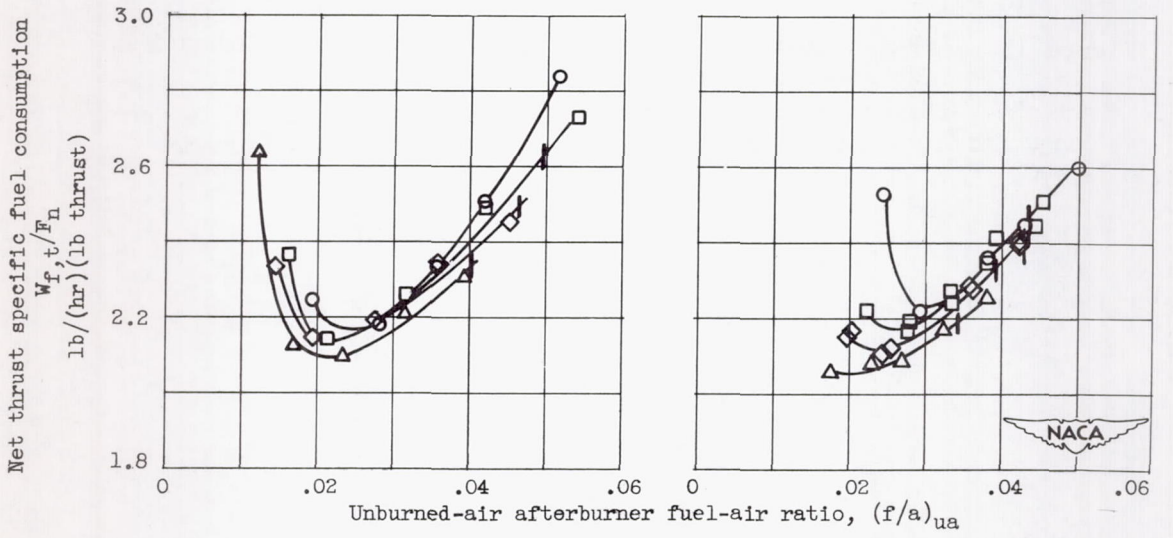

(b) Net thrust specific fuel consumption.

Figure 16. - Variation of over-all afterburner performance with afterburner fuel-air ratio at several flight Mach numbers.

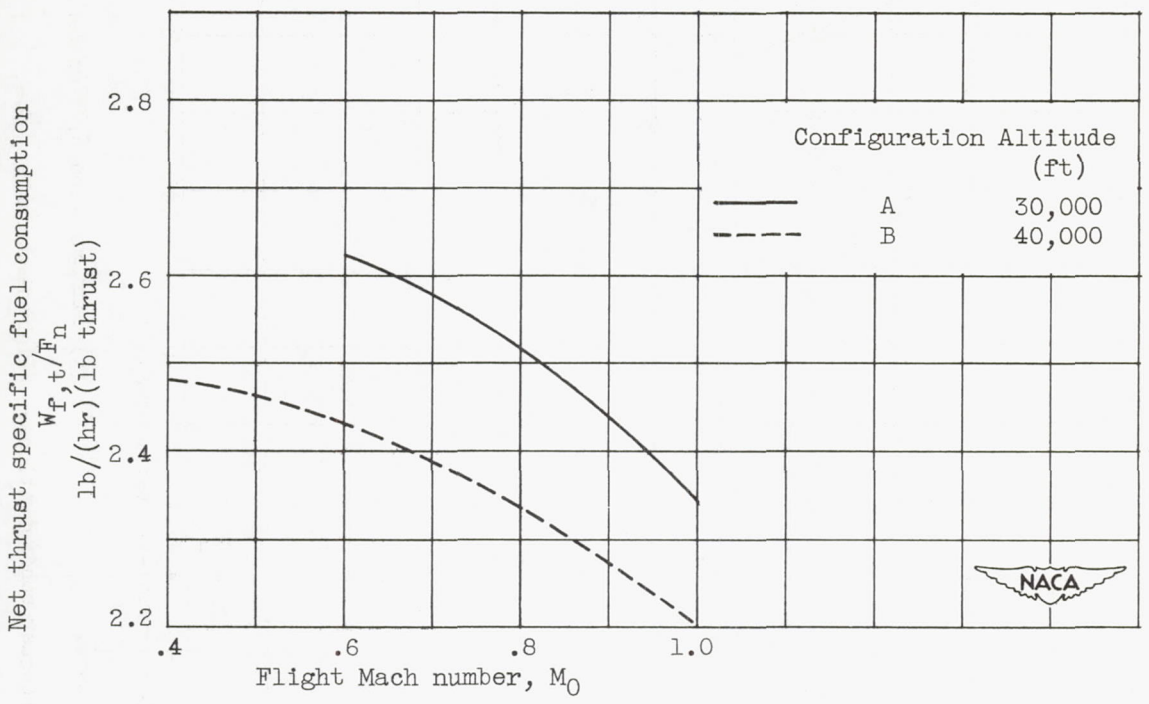

Figure 17. - Effect of flight Mach number on net thrust specific fuel consumption at rated turbine-outlet total temperature and engine speed.

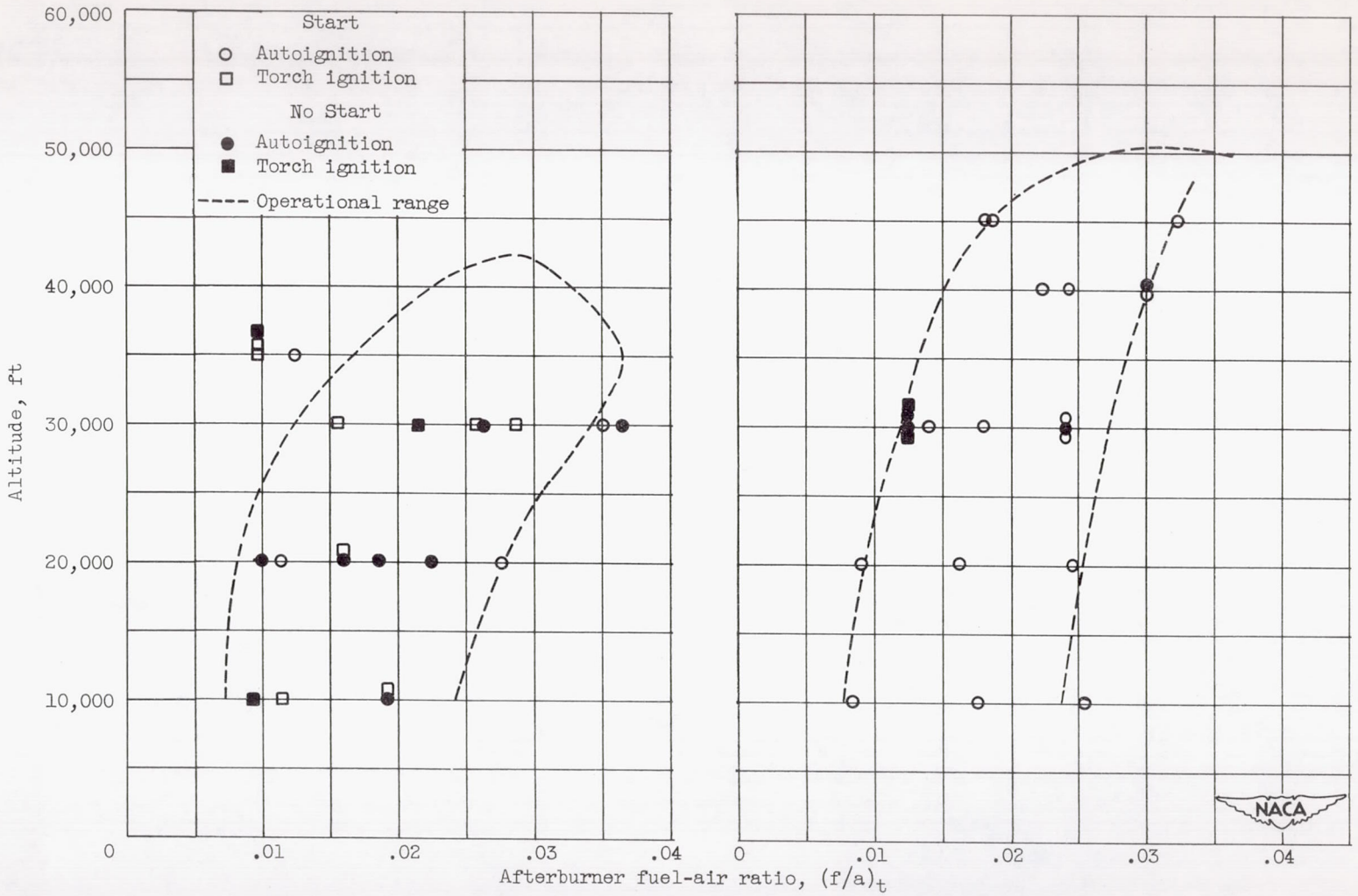

(a) Configuration A, H- and V-gutters.

(b) Configuration B, V-gutter.

Figure 18. - Starting range of afterburner configurations. Flight Mach number, 0.6.